Article

MMS

Mathematics and Mechanics of Solids
1–21

DOI: 10.1177/1081286516666133
mms.sagepub.com
SAGE

Singular asymptotic expansion of the elastic solution along an edge around which material properties depend on the angular coordinate

Netta Omer
Department of Mechanical Engineering, Afeka College of Engineering, Tel Aviv, Israel

Zohar Yosibash
Department of Mechanical Engineering, Ben-Gurion University of the Negev, Beer-Sheva, Israel

Received 28 May 2015; accepted 5 April 2016

Abstract
The solution to the elasticity problem in three-dimensional polyhedral domains in the vicinity of an edge around which the material properties depend on the angular angle is addressed. This asymptotic solution involves a family of eigenpairs and their shadows which are being computed by means of p-finite element methods. In particular the examples we give explicitly provide the asymptotic solution for cracks and V-notch edges and explore the eigenvalues as a function of the change in material properties in the angular direction. We demonstrate that the singular exponents may change considerably by changing the material properties variation in the angular direction. These eigenpairs are necessary to allow the extraction of the edge stress intensity functions.

Keywords
Edge stress intensity functions, high order finite elements, composite materials, fracture mechanics, elasticity

1. Introduction

Solutions to linear elastic problems in three-dimensional (3-D) polygonal domains in the vicinity of reentrant edges, when the material properties in the vicinity of the edges are constant or piecewise constant were studied in the work by Omer and Yosibash [1–3]. These are described in terms of special singular functions (eigenfunctions) depending on the geometry and the boundary conditions in the vicinity of the edge on one hand, and of the unknown function of the coordinate along the edge (edge stress intensity functions) depending on the given body forces and tractions on the other hand. The eigenpairs (eigenvalues and eigenfunctions) may be obtained by several techniques. An analytical method for computing eigenpairs in isotropic two-dimensional (2-D) domains is provided in many prior publications [4–7]. A semi-analytic approach for the eigenpairs computations was presented by Costabel et al. [8], applicable to anisotropic domains. Many numerical methods were developed, as for example in the work by Leguillon and Sanches-Palencia, Szabó and Yosibash [9–12], which are applicable also to anisotropic and multi-material interfaces. Many publications have focused in the past few decades on the 3-D effects in cracks and notches. A review of the development in this field is presented by Pook [13].

Corresponding author:
Netta Omer, Department of Mechanical Engineering, Afeka College of Engineering, Tel-Aviv, 6998812, Israel.
Email: NettaO@afeka.ac.il

Most of past studies on singularities address homogenous materials. However recent materials like functional graded materials (FGM) are manufactured so that the material properties, although isotropic, change continuously in the material (the elastic modulus, E, for example changes smoothly as a function of a coordinate). For future application of the methods to determine the singular solution in the vicinity of a crack edge in FGM materials, we started with a more simplified model in which the elastic modulus changes continuously as a function of one coordinate (the angular axis, θ).

The smallest eigenvalues of the singular asymptotic solutions for 2-D cracked domains may even be as small as $(0+\varepsilon)$ for specific mixed boundary conditions ([12, 14, 15]). The strain energy density (stress $\times$ strain) for such cases behaves as $r^{(-2+2\varepsilon)}$ and involves an integral over an area which must include an integral over r, where $r \geq 0$; i.e. the integral is of the form: $r^{(-2+2\varepsilon)}rdrd\theta$ and therefore the constrain in ε becomes $\varepsilon > 0$.

The aim of this paper is to investigate the asymptotic solution in the vicinity of singular edges at which the material properties change continuously or piecewise continuously as a function of the angular axis θ. The singularity exponents in the asymptotic solution are sensitive to the material properties variation, and may obtain values considerably smaller than $1/2$ (the crack exponent in homogeneous isotropic materials) depending on the angular variation of Young's modulus for example. We also demonstrate that the tangential variation of the material properties result in a coupled mode situation, so that Mode I and Mode II edge stress intensity functions become coupled, although the loading conditions are pure Mode I or pure Mode II.

We derive the weak formulation for the computation of the eigenpairs (that construct the asymptotic expansion) and discretize this formulation so to allow the use the p-version of the finite element method (FEM) [16]. Numerical examples are then considered that demonstrate the dependence of the eigenvalues (singularity exponents) on the variation of the material properties.

The paper is organized as follows. We start with notations, defining the domain of interest and the linear elastic problem in the vicinity of an edge, and it's reduction to a 1-D problem for the computation of the eigenpairs. A mathematical algorithm is then presented for computing the eigen-pairs and the associated eigenfunctions and shadows. The p-finite element (FE) formulation is thereafter addressed, based on which numerical discretization of the continuous problem is applied. Finally, several numerical tests are presented which demonstrate the accuracy and efficiency of the presented methods. Specifically we compute the eigenpairs and eigenstresses associated with traction free boundary conditions for a cracked and a V-notched domain with material properties which vary quadratically in θ. Both symmetric and anti-symmetric material properties in θ are considered. We finish with a summary and conclusions section.

2. The elastic solution for an isotropic problem in the vicinity of an edge

In this section we derive the asymptotic solution in the neighborhood of an edge in an isotropic elastic domain having material properties depending on the angular angle. The material properties are isotropic but inhomogeneous. This means that at each point in the domain the mechanical response in each direction is the same, but in two different points in the domain the material properties differ. It is shown that the elastic solution can be presented as an asymptotic series of eigenpairs (the well known eigen-pairs of the 2-D cross section), shadows and the associated edge stress intensity functions. We follow the steps presented by Omer and Yosibash [1] and expand it to θ dependent material properties.

2.1. Notations and the differential equations

Consider a domain Ω in which one straight edge $\mathcal{E}$ of interest is present. The domain is generated as the product $\Omega = G \times I$ where I is the interval $[-1, 1]$ and G is a plane bounded sector of opening $\omega \in (0, 2\pi]$, for simplicity let us assume it has a radius 1 (the case of a crack, $\omega = 2\pi$, is included), as shown in Figure 1. Although any G or I can be chosen, these simplified ones have been chosen for simplicity of presentation.

The variables in G and I are (x_1, x_2) and x_3 respectively, and the coordinates (x_1, x_2, x_3) are denoted by $\boldsymbol{x}$. Let (r, θ) be the polar coordinates centered at the vertex of G, so that G coincides with $\{(x_1, x_2) \in \mathbb{R}^2 \mid r \in (0, 1),\ \theta \in (0, \omega)\}$. The edge $\mathcal{E}$ of interest is the set $\{\boldsymbol{x} \in \mathbb{R}^3 \mid r = 0,\ x_3 \in I\}$. The two flat planes that intersect at the edge $\mathcal{E}$ are denoted by Γ_1 and Γ_2.

Remark 1 *The methods presented in this paper are restricted to geometries where the edges are straight lines and the angle ω is fixed along x_3.*

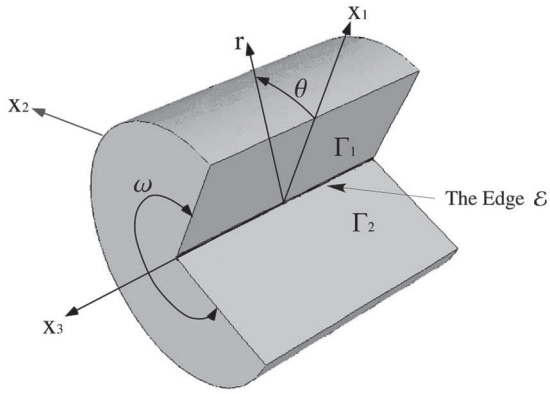

Figure 1. Domain of interest Ω.

Remark 2 *In general the eigenpairs associated with the elasticity operator may be complex, but in most practical cases the eigenvalues smaller than* 1 *are of interest, and these are usually real. Herein we address real eigenpairs only, whereas the general case will be addressed in a future publication.*

The displacements vector in the polar coordinates is considered here, denoted $\tilde{\boldsymbol{u}} = \{u_r, u_\theta, u_{x_3}\}^{\mathrm{T}}$. With this notation, the Navier-Lamé equations that describe the elastic isotropic problem in polar coordinates are

$$\begin{gathered}(\lambda+2\mu)(\partial_r^2 u_r + \tfrac{1}{r}\partial_r u_r - \tfrac{1}{r^2}u_r) + \tfrac{1}{r^2}\mu\partial_\theta^2 u_r + \tfrac{1}{r^2}\tfrac{d\mu}{d\theta}\partial_\theta u_r + \mu\partial_3^2 u_r \\ -\tfrac{1}{r^2}(\lambda+3\mu)\partial_\theta u_\theta + \tfrac{1}{r}(\lambda+\mu)\partial_r\partial_\theta u_\theta - \tfrac{1}{r^2}\tfrac{d\mu}{d\theta}u_\theta + \tfrac{1}{r}\tfrac{d\mu}{d\theta}\partial_r u_\theta \\ +(\lambda+\mu)\partial_r\partial_3 u_3 = 0,\end{gathered} \tag{1}$$

$$\begin{gathered}\tfrac{1}{r}(\lambda+\mu)\partial_r\partial_\theta u_r + \tfrac{1}{r^2}(\lambda+3\mu)\partial_\theta u_r + \tfrac{1}{r}\tfrac{d\lambda}{d\theta}\partial_r u_r + \tfrac{1}{r^2}(\tfrac{d\lambda}{d\theta}+2\tfrac{d\mu}{d\theta})u_r \\ +\mu(\partial_r^2 + \tfrac{1}{r}\partial_r - \tfrac{1}{r^2})u_\theta + \tfrac{1}{r^2}(\lambda+2\mu)\partial_\theta^2 u_\theta + \tfrac{1}{r^2}(\tfrac{d\lambda}{d\theta}+2\tfrac{d\mu}{d\theta})\partial_\theta u_\theta + \mu\partial_3^2 u_\theta \\ \tfrac{1}{r}(\lambda+\mu)\partial_\theta\partial_3 u_3 + \tfrac{1}{r}\tfrac{d\lambda}{d\theta}\partial_3 u_3 = 0,\end{gathered} \tag{2}$$

$$\begin{gathered}(\lambda+\mu)\partial_r\partial_3 u_r + \tfrac{1}{r}(\lambda+\mu)\partial_3 u_r + \tfrac{1}{r}(\lambda+\mu)\partial_\theta\partial_3 u_\theta + \tfrac{1}{r}\tfrac{d\mu}{d\theta}\partial_3 u_\theta \\ \mu(\partial_r^2 + \tfrac{1}{r}\partial_r + \tfrac{1}{r^2}\partial_\theta^2)u_3 + (\lambda+2\mu)\partial_3^2 u_3 + \tfrac{1}{r^2}\tfrac{d\mu}{d\theta}\partial_\theta u_3 = 0.\end{gathered} \tag{3}$$

with $\lambda = \lambda(\theta), \mu = \mu(\theta)$ being the Lamé functions associated with the engineering material $E(\theta)$, the Young's modulus and $\nu(\theta)$ the Poisson ratio. For convenience of notation we define

$$\beta_k(\theta) = \lambda(\theta) + k\mu(\theta).$$

We follow the same steps as in the article by Omer and Yosibash [1] to allow the consideration of a solution $\tilde{\boldsymbol{u}}$ of the form

$$\tilde{\boldsymbol{u}} = \sum_{j\geq 0} \partial_3^j A(x_3)\boldsymbol{\Phi}_j(r,\theta). \tag{4}$$

The 3-D problem given by equations (1) to (3) is reduced to a system of 2-D partial differential equations (PDEs) on a 2-D domain G for the determination of the functions $\boldsymbol{\Phi}_j(r,\theta)$

$$\begin{cases}[M_0]\boldsymbol{\Phi}_0 = 0 \\ [M_0]\boldsymbol{\Phi}_1 + [M_1]\boldsymbol{\Phi}_0 = 0 \\ [M_0]\boldsymbol{\Phi}_{j+2} + [M_1]\boldsymbol{\Phi}_{j+1} + [M_2]\boldsymbol{\Phi}_j = 0, \ \ j \geq 0\end{cases} \qquad (r,\theta) \in G, \tag{5}$$

where

$$[M_0] = \begin{pmatrix} \beta_2 K_r^{\partial} + \frac{1}{r^2}\mu\partial_\theta^2 + \frac{1}{r^2}\frac{d\mu}{d\theta}\partial_\theta & -\frac{1}{r^2}\beta_3\partial_\theta + \frac{1}{r}\beta_1\partial_r\partial_\theta - \frac{1}{r^2}\frac{d\mu}{d\theta} + \frac{1}{r}\frac{d\mu}{d\theta}\partial_r & 0 \\ \frac{1}{r}\beta_1\partial_r\partial_\theta + \frac{1}{r^2}\beta_3\partial_\theta + \frac{1}{r}\frac{d\lambda}{d\theta}\partial_r + \frac{1}{r^2}K_{\lambda,\mu}^{\partial} & \mu K_r^{\partial} + \frac{1}{r^2}\beta_2\partial_\theta^2 + \frac{1}{r^2}K_{\lambda,\mu}^{\partial}\partial_\theta & 0 \\ 0 & 0 & \mu K_{r,\theta}^{\partial} + \frac{1}{r^2}\frac{d\mu}{d\theta} \end{pmatrix},$$

$$[M_1] = \begin{pmatrix} 0 & 0 & \beta_1\partial_r \\ 0 & 0 & \frac{1}{r}\beta_1\partial_\theta + \frac{1}{r}\frac{d\lambda}{d\theta} \\ \beta_1\partial_r + \frac{1}{r}\beta_1 & \frac{1}{r}\beta_1\partial_\theta + \frac{1}{r}\frac{d\mu}{d\theta} & 0 \end{pmatrix}, \qquad [M_2] = \begin{pmatrix} \mu & 0 & 0 \\ 0 & \mu & 0 \\ 0 & 0 & \beta_2 \end{pmatrix}, \tag{6}$$

with

$$K_r^{\partial} = (\partial_r^2 + \frac{1}{r}\partial_r - \frac{1}{r^2}), \qquad K_{r,\theta}^{\partial} = (\partial_r^2 + \frac{1}{r}\partial_r + \frac{1}{r^2}\partial_\theta^2), \qquad K_{\lambda,\mu}^{\partial} = (\frac{d\lambda}{d\theta} + 2\frac{d\mu}{d\theta}). \tag{7}$$

accompanied by homogeneous boundary conditions on the two surfaces Γ_1 and Γ_2, discussed in the sequel.

By investigating the structure of the system of PDEs given by equation (5), we show in the next section how to reduce these to a much simpler system of ordinary differential equations (ODEs) in one dimension. To this end, we note that the first PDE in equation (5) generates the solution $\mathbf{\Phi}_0$ associated with the eigenvalue α, denoted *primal singular function*, which is the well known eigenfunction for a 2-D problem on the cross-section G

$$\mathbf{\Phi}_0 = r^{\alpha}\boldsymbol{\varphi}_0(\theta). \tag{8}$$

All $\mathbf{\Phi}_j, j \geq 1$ are called *shadow functions* of the primal singular function $\mathbf{\Phi}_0$:

$$\mathbf{\Phi}_j = r^{\alpha+j}\boldsymbol{\varphi}_j(\theta), \tag{9}$$

where $\mathbf{\Phi}_1$ is the solution of the second PDE in equation (5) and sequence $\mathbf{\Phi}_j$ (where $j \geq 2$) are the solutions of the third recursive equation given in equation (5). There exist an infinite number of shadow functions $\mathbf{\Phi}_j$ for each eigenvalue α_i (these are obtained by applying boundary conditions as will be discussed in Subsection 2.2)

$$\mathbf{\Phi}_j^{(\alpha_i)} = r^{\alpha_i+j}\boldsymbol{\varphi}_j^{(\alpha_i)}(\theta) \quad j = 0, 1, \ldots \tag{10}$$

Thus, for each eigenvalue α_i, the 3-D solution, in the vicinity of an edge is

$$\tilde{\boldsymbol{u}}^{(\alpha_i)} = \sum_{j\geq 0} \partial_3^j A_i(x_3) r^{\alpha_i+j}\boldsymbol{\varphi}_j^{(\alpha_i)}(\theta) \tag{11}$$

and the overall solution $\tilde{\boldsymbol{u}}$ is

$$\tilde{\boldsymbol{u}} = \sum_{i\geq 1} \tilde{\boldsymbol{u}}^{(\alpha_i)} = \sum_{i\geq 1}\sum_{j\geq 0} \partial_3^j A_i(x_3) r^{\alpha_i+j}\boldsymbol{\varphi}_j^{(\alpha_i)}(\theta), \tag{12}$$

where $A_i(x_3)$ is the edge stress intensity function (ESIF) of the ith eigenvalue.

Because the operator $\mathcal{L}$ is self-adjoint, for any real eigenvalue α_i the number $-\alpha_i$ is also an eigenvalue. It is associated with an eigenfunction $\mathbf{\Phi}_0^{(-\alpha_i)}$ and its shadows $\mathbf{\Phi}_j^{(-\alpha_i)}$ by similar formulas as in equation (10). Solutions of equation (5) for the *negative eigenvalues* $-\alpha_i$ are called the *dual singular solutions*, and are denoted by $\mathbf{\Psi}_j^{(\alpha_i)}$. For normalization purposes, a real coefficient $c_0^{(\alpha_i)}$ is chosen, linking $\mathbf{\Phi}_j^{(-\alpha_i)}$ with $\mathbf{\Psi}_j^{(\alpha_i)}$:

$$\mathbf{\Psi}_0^{(\alpha_i)} = r^{-\alpha_i}\boldsymbol{\psi}_0^{(\alpha_i)}(\theta) = c_0^{(\alpha_i)} r^{-\alpha_i}\boldsymbol{\varphi}_0^{(-\alpha_i)}(\theta) \tag{13}$$

and

$$\mathbf{\Psi}_j^{(\alpha_i)} = r^{-\alpha_i+j}\boldsymbol{\psi}_j^{(\alpha_i)}(\theta) = c_0^{(\alpha_i)} r^{-\alpha_i+j}\boldsymbol{\varphi}_j^{(-\alpha_i)}(\theta). \tag{14}$$

The eigenpairs and their shadows, as well as the dual functions and shadows for constant or piecewise constant material properties, with rigorous mathematical formulations are provided in the work by Costabel et al. [17] and engineering examples with a detailed explanation about the shadow functions, their computation and the GESIFs are available in the work by Yosibash et al. [12, 18].

2.2. Boundary condition for the primal and dual shadow functions

Traction free boundary conditions are considered on Γ_1 and Γ_2 surfaces

$$[T](\tilde{\boldsymbol{u}})|_{\Gamma_1,\Gamma_2} = ([T_0(\partial_r,\partial_\theta)]\tilde{\boldsymbol{u}} + [T_1(\partial_r,\partial_\theta)]\partial_3\tilde{\boldsymbol{u}})\,|_{\Gamma_1,\Gamma_2} = 0. \tag{15}$$

Inserting equation (4) in to equation (15) one obtains

$$A(x_3)[T_0]\boldsymbol{\Phi}_0|_{\Gamma_1,\Gamma_2} + \sum_{j\geq 0}\partial_3^{j+1}A(x_3)\left([T_0]\boldsymbol{\Phi}_{j+1} + [T_1]\boldsymbol{\Phi}_j\right)|_{\Gamma_1,\Gamma_2} = 0. \tag{16}$$

Equation (16) has to hold for any smooth function $A(x_3)$ and therefore the boundary conditions for the eigenfunctions are

$$\begin{cases} [T_0]\boldsymbol{\Phi}_0 = 0 \\ [T_0]\boldsymbol{\Phi}_{j+1} + [T_1]\boldsymbol{\Phi}_j = 0,\ \ j \geq 0 \end{cases} \qquad \text{on} \quad \Gamma_1, \Gamma_2. \tag{17}$$

The first part of equation (17) is the boundary condition for $\boldsymbol{\Phi}_0$ which is identical to the 2-D boundary conditions. The second part in equation (17) is the boundary condition for each $\boldsymbol{\Phi}_j$ where $j \geq 1$. The operator-matrices $[T_0]$ and $[T_1]$ are explicitly derived from

$$\begin{cases} (\sigma_{r\theta})\,|_{\theta=0,\omega} = 0 \\ (\sigma_{\theta\theta})\,|_{\theta=0,\omega} = 0 \\ (\sigma_{\theta 3})\,|_{\theta=0,\omega} = 0 \end{cases} \quad \Rightarrow \quad \begin{cases} \left(\mu\left(\frac{1}{r}\partial_\theta u_r + \partial_r u_\theta - \frac{1}{r}u_\theta\right)\right)|_{\theta=0,\omega} = 0 \\ \left(\beta_2\frac{1}{r}u_r + \lambda\partial_r u_r + \beta_2\frac{1}{r}\partial_\theta u_\theta + \lambda\partial_3 u_3\right)|_{\theta=0,\omega} = 0 \\ \left(\mu\left(\partial_3 u_\theta + \frac{1}{r}\partial_\theta u_3\right)\right)|_{\theta=0,\omega} = 0 \end{cases}$$

obtaining

$$[T_0] = \begin{pmatrix} \mu\frac{1}{r}\partial_\theta & \mu\partial_r - \mu\frac{1}{r} & 0 \\ \beta_2\frac{1}{r} + \lambda\partial_r & \beta_2\frac{1}{r}\partial_\theta & 0 \\ 0 & 0 & \mu\frac{1}{r}\partial_\theta \end{pmatrix}, \qquad [T_1] = \begin{pmatrix} 0 & 0 & 0 \\ 0 & 0 & \lambda \\ 0 & \mu & 0 \end{pmatrix}. \tag{18}$$

3. The weak formulation for the computation of eigenpairs

3.1. The primal eigenpair α and $\boldsymbol{\Phi}_0$

Any eigenvalue α and primal eigenfunction $r^\alpha\boldsymbol{\varphi}_0^{(\alpha)}$, (and dual eigenfunctions $r^{-\alpha}\boldsymbol{\psi}_0^{(\alpha)}$) are the solution of the first part in equation (5). One may notice that after substituting $r^\alpha\boldsymbol{\varphi}_0^{(\alpha)}$ for $\boldsymbol{\Phi}_0$ the dependency on r disappears, and an ODE in θ has to be solved

$$[A_1^0]\boldsymbol{\varphi}_0'' + \left(\alpha[A_2^0] + [A_3^0] + [D_3^0]\right)\boldsymbol{\varphi}_0' + \left(\alpha^2[A_4^0] + \alpha[D_5^0] + [A_6^0] + [D_6^0]\right)\boldsymbol{\varphi}_0 = 0, \quad \theta \in (0,\omega), \tag{19}$$

which is a quadratic eigenvalue problem. The matrices $[A_i^0], [D_i^0]$ are composed of the material properties

$$[A_1^0] = \begin{pmatrix} \mu & 0 & 0 \\ 0 & \beta_2 & 0 \\ 0 & 0 & -\mu \end{pmatrix}, \quad [A_2^0] = \begin{pmatrix} 0 & \beta_1 & 0 \\ \beta_1 & 0 & 0 \\ 0 & 0 & 0 \end{pmatrix}, \quad [A_3^0] = \begin{pmatrix} 0 & -\beta_3 & 0 \\ \beta_3 & 0 & 0 \\ 0 & 0 & 0 \end{pmatrix},$$
$$[A_4^0] = \begin{pmatrix} \beta_2 & 0 & 0 \\ 0 & \mu & 0 \\ 0 & 0 & -\mu \end{pmatrix}, \quad [A_6^0] = \begin{pmatrix} -\beta_2 & 0 & 0 \\ 0 & -\mu & 0 \\ 0 & 0 & 0 \end{pmatrix}, \tag{20}$$
$$[D_3^0] = \begin{pmatrix} \frac{d\mu}{d\theta} & 0 & 0 \\ 0 & (\frac{d\lambda}{d\theta} + 2\frac{d\mu}{d\theta}) & 0 \\ 0 & 0 & -\frac{d\mu}{d\theta} \end{pmatrix}, \quad [D_5^0] = \begin{pmatrix} 0 & \frac{d\mu}{d\theta} & 0 \\ \frac{d\lambda}{d\theta} & 0 & 0 \\ 0 & 0 & 0 \end{pmatrix}, \quad [D_6^0] = \begin{pmatrix} 0 & -\frac{d\mu}{d\theta} & 0 \\ (\frac{d\lambda}{d\theta} + 2\frac{d\mu}{d\theta}) & 0 & 0 \\ 0 & 0 & 0 \end{pmatrix}.$$

The ODE (19) is complemented by traction free boundary conditions from equation $(17)_1$

$$\left\{[B_1^0]\boldsymbol{\varphi}_0' + \left(\alpha[B_2^0] + [B_3^0]\right)\boldsymbol{\varphi}_0\right\}_{\theta=0,\omega} = 0, \tag{21}$$

where

$$[B_1^0] = [A_1^0], \quad [B_2^0] = \begin{pmatrix} 0 & \mu & 0 \\ \lambda & 0 & 0 \\ 0 & 0 & 0 \end{pmatrix}, \quad [B_3^0] = \begin{pmatrix} 0 & -\mu & 0 \\ \beta_2 & 0 & 0 \\ 0 & 0 & 0 \end{pmatrix}. \tag{22}$$

To obtain a weak formulation that may be solved by the FE method we multiply equation (19) by a test function $\boldsymbol{v}$, integrate over $0 \le \theta \le \omega$ and use integration by parts for the second derivative term to obtain

$$\begin{aligned} &\left\{\left\{[A_1^0]\boldsymbol{\varphi}_0'\right\}^{\mathrm{T}}\boldsymbol{v}\right\}_{\theta=0,\omega} - \int_0^\omega \left\{[A_1^0]\boldsymbol{\varphi}_0'\right\}^{\mathrm{T}}\boldsymbol{v}'d\theta - \int_0^\omega \left\{\tfrac{d[A_1^0]}{d\theta}\boldsymbol{\varphi}_0'\right\}^{\mathrm{T}}\boldsymbol{v}'d\theta \\ &+ \int_0^\omega \left\{\left(\alpha[A_2^0] + [A_3^0] + [D_3^0]\right)\boldsymbol{\varphi}_0'\right\}^{\mathrm{T}}\boldsymbol{v}d\theta + \int_0^\omega \left\{\left(\alpha^2[A_4^0] + \alpha[D_5^0] + [A_6^0] + [D_6^0]\right)\boldsymbol{\varphi}_0\right\}^{\mathrm{T}}\boldsymbol{v}d\theta = 0. \end{aligned} \tag{23}$$

Noticing that $\frac{d[A_1^0]}{d\theta} = [D_3^0]$ and $[A_1^0] = [B_1^0]$ we obtain

$$\begin{aligned} &-\alpha\left\{\left\{[B_2^0]\boldsymbol{\varphi}_0\right\}^{\mathrm{T}}\boldsymbol{v}\right\}|_{\theta=0,\omega} - \left\{\left\{[B_3^0]\boldsymbol{\varphi}_0\right\}^{\mathrm{T}}\boldsymbol{v}\right\}|_{\theta=0,\omega} - \int_0^\omega \left\{[A_1^0]\boldsymbol{\varphi}_0'\right\}^{\mathrm{T}}\boldsymbol{v}'d\theta \\ &+ \int_0^\omega \left\{\left(\alpha[A_2^0] + [A_3^0]\right)\boldsymbol{\varphi}_0'\right\}^{\mathrm{T}}\boldsymbol{v}d\theta + \int_0^\omega \left\{\left(\alpha^2[A_4^0] + \alpha[D_5^0] + [A_6^0] + [D_6^0]\right)\boldsymbol{\varphi}_0\right\}^{\mathrm{T}}\boldsymbol{v}d\theta = 0. \end{aligned} \tag{24}$$

The weak eigen-formulation for the primal and dual eigenpairs is therefore

$$\boxed{\begin{aligned} &\text{Seek} \quad \alpha \in \mathbb{C}, \quad 0 \neq \boldsymbol{\varphi}_0 \in H^1(0,\omega), \quad \text{s.t.} \quad \forall \boldsymbol{v} \in H^1(0,\omega) \\ &\mathcal{B}_0^0(\boldsymbol{\varphi}_0,\boldsymbol{v}) + \alpha\mathcal{B}_1^0(\boldsymbol{\varphi}_0,\boldsymbol{v}) + \alpha^2\mathcal{B}_2^0(\boldsymbol{\varphi}_0,\boldsymbol{v}) = 0 \end{aligned}} \tag{25}$$

where H^1 is the Sobolev space and

$$\begin{aligned} \mathcal{B}_0^0(\boldsymbol{\varphi}_0,\boldsymbol{v}) &= -\left\{\left\{[B_3^0]\boldsymbol{\varphi}_0\right\}^{\mathrm{T}}\boldsymbol{v}\right\}|_{\theta=0,\omega} - \int_0^\omega \left\{[A_1^0]\boldsymbol{\varphi}_0'\right\}^{\mathrm{T}}\boldsymbol{v}'d\theta + \int_0^\omega \left\{[A_3^0]\boldsymbol{\varphi}_0'\right\}^{\mathrm{T}}\boldsymbol{v}d\theta \\ &\quad + \int_0^\omega \left\{[A_6^0]\boldsymbol{\varphi}_0\right\}^{\mathrm{T}}\boldsymbol{v}d\theta + \int_0^\omega \left\{[D_6^0]\boldsymbol{\varphi}_0\right\}^{\mathrm{T}}\boldsymbol{v}d\theta \\ \mathcal{B}_1^0(\boldsymbol{\varphi}_0,\boldsymbol{v}) &= -\left\{\left\{[B_2^0]\boldsymbol{\varphi}_0\right\}^{\mathrm{T}}\boldsymbol{v}\right\}|_{\theta=0,\omega} + \int_0^\omega \left\{[A_2^0]\boldsymbol{\varphi}_0'\right\}^{\mathrm{T}}\boldsymbol{v}d\theta + \int_0^\omega \left\{[D_5^0]\boldsymbol{\varphi}_0\right\}^{\mathrm{T}}\boldsymbol{v}d\theta \\ \mathcal{B}_2^0(\boldsymbol{\varphi}_0,\boldsymbol{v}) &= \int_0^\omega \left\{[A_4^0]\boldsymbol{\varphi}_0\right\}^{\mathrm{T}}\boldsymbol{v}d\theta. \end{aligned} \tag{26}$$

3.1.1. p-FEMs for the primal eigenpair α and $\boldsymbol{\varphi}_0$ We apply p-FEMs for the solution of equation (25). To this end $\boldsymbol{\varphi}_0 = \begin{pmatrix} u_0 & v_0 & w_0 \end{pmatrix}^{\mathrm{T}}$ is expressed in terms of the basis functions $N_k(\xi)$ (integrals of Legendre polynomials) in the standard element

$$u_0(\xi) = \sum_{k=1}^{p+1} a_k N_k(\xi), \quad v_0(\xi) = \sum_{k=1}^{p+1} a_{p+1+k} N_k(\xi), \quad w_0(\xi) = \sum_{k=1}^{p+1} a_{2p+2+k} N_k(\xi) \tag{27}$$

or

$$\boldsymbol{\varphi}_0 = \begin{pmatrix} N_1(\xi)\cdots N_{p+1}(\xi) & 0\cdots 0 & 0\cdots 0 \\ 0\cdots 0 & N_1(\xi)\cdots N_{p+1}(\xi) & 0\cdots 0 \\ 0\cdots 0 & 0\cdots 0 & N_1(\xi)\cdots N_{p+1}(\xi) \end{pmatrix} \begin{pmatrix} a_1 \\ \vdots \\ a_{3(p+1)} \end{pmatrix} \stackrel{\text{def}}{=} [N]\boldsymbol{a}_0. \tag{28}$$

Similarly $\boldsymbol{v} \overset{\text{def}}{=} [N]\boldsymbol{b}_0$, and $d\theta = \frac{\omega}{2} d\xi$. Substituting equation (28) in to equation (25) one obtains the FE formulation of the weak eigen-form

$$\boldsymbol{a}_0^{\mathrm{T}} \left(\alpha^2 [K_2^0] + \alpha [K_1^0] + [K_0^0] \right) = \vec{0}, \tag{29}$$

where

$$\begin{aligned}
[K_2^0] &= \tfrac{\omega}{2} \textstyle\int_{-1}^{1} [N]^{\mathrm{T}} [A_4^0]^{\mathrm{T}} [N] d\xi \\
[K_1^0] &= -\left\{ [N]^{\mathrm{T}} [B_2^0]^{\mathrm{T}} [N] \right\}_{\theta=0,\omega} + \textstyle\int_{-1}^{1} [N']^{\mathrm{T}} [A_2^0]^{\mathrm{T}} [N] d\xi + \tfrac{\omega}{2} \int_{-1}^{1} [N]^{\mathrm{T}} [D_5^0]^{\mathrm{T}} [N] d\xi \\
[K_0^0] &= -\left\{ [N]^{\mathrm{T}} [B_3^0]^{\mathrm{T}} [N] \right\}_{\theta=0,\omega} - \tfrac{2}{\omega} \textstyle\int_{-1}^{1} [N']^{\mathrm{T}} [A_1^0]^{\mathrm{T}} [N'] d\xi + \int_{-1}^{1} [N']^{\mathrm{T}} [A_3^0]^{\mathrm{T}} [N] d\xi \\
&\quad + \tfrac{\omega}{2} \textstyle\int_{-1}^{1} [N]^{\mathrm{T}} [A_6^0]^{\mathrm{T}} [N] d\xi + \tfrac{\omega}{2} \int_{-1}^{1} [N]^{\mathrm{T}} [D_6^0]^{\mathrm{T}} [N] d\xi .
\end{aligned} \tag{30}$$

The quadratic matrix eigen-problem given by equation (29) is solved by a proper linearization process, see the following reference [19]. Setting $\boldsymbol{d}_0 = \alpha \boldsymbol{a}_0$, the $(3p+3) \times (3p+3)$ quadratic eigen-problem is transformed into a linear $(6p+6) \times (6p+6)$ "standard matrix eigen-problem":

$$\begin{pmatrix} \boldsymbol{a}_0 \\ \boldsymbol{d}_0 \end{pmatrix}^{\mathrm{T}} \begin{pmatrix} 0 & [K_0^0] \\ I & [K_1^0] \end{pmatrix} = \alpha \begin{pmatrix} \boldsymbol{a}_0 \\ \boldsymbol{d}_0 \end{pmatrix}^{\mathrm{T}} \begin{pmatrix} I & 0 \\ 0 & -[K_2^0] \end{pmatrix}. \tag{31}$$

Remark 3 *The method presented in this section addresses $\boldsymbol{\varphi}_0$ as well as $\boldsymbol{\psi}_0$. The positive values of the eigenvalue α obtained from equation* (29) *are associated with the eigenfunction $\boldsymbol{\varphi}_0$, whereas the negative values of α are associated with the dual eigenfunction $\boldsymbol{\psi}_0$.*

3.2. The first shadow function, $\boldsymbol{\varphi}_1$

The shadow functions $\boldsymbol{\varphi}_1$, presented in equation (12), as well as the dual shadow function $\boldsymbol{\psi}_1$ are the solution of the second differential equation in equation (5).

Remark 4 *Although it seems that the method presented herein addresses $\boldsymbol{\varphi}_1$, it is equally applicable to $\boldsymbol{\psi}_1$ by replacing $\boldsymbol{\varphi}_1$, $\boldsymbol{\varphi}_0$ and α by $\boldsymbol{\psi}_1$, $\boldsymbol{\psi}_0$ and $-\alpha$. Notice that the eigenvalue α is known so the unknown functions $\boldsymbol{\varphi}_1$ and $\boldsymbol{\psi}_1$ are obtained by solving equation* $(5)_2$.

Substituting $r^{\alpha} \boldsymbol{\varphi}_0^{(\alpha)}$ for $\boldsymbol{\Phi}_0$ and $r^{\alpha+1} \boldsymbol{\varphi}_1^{(\alpha)}$ for $\boldsymbol{\Phi}_1$ in equation $(5)_2$, the dependency on r disappears, and an ODE in θ is to be solved:

$$\begin{aligned}
&[A_1^0] \boldsymbol{\varphi}_1'' + \left(\alpha [A_2^0] + [A_3^1] + [D_3^0] \right) \boldsymbol{\varphi}_1' + \left(\alpha^2 [A_4^0] + \alpha ([A_5^1] + [D_5^0]) + [A_6^1] + [D\,{}_6^1] \right) \boldsymbol{\varphi}_1 \\
&\quad + [A_7^1] \boldsymbol{\varphi}_0' + \left(\alpha [A_8^1] + [A_9^1] + [D_9^1] \right) \boldsymbol{\varphi}_0 = \vec{0}.
\end{aligned} \tag{32}$$

The matrices $[A_i^1]$ depend on the material constants

$$\begin{aligned}
&[A_3^1] = [A_3^0] + [A_2^0], \quad [A_5^1] = 2[A_4^0], \quad [A_6^1] = [A_6^0] + [A_4^0], \quad [D\,{}_6^1] = [D\,{}_6^0] + [D_5^0] \\
&[A_7^1] = \begin{pmatrix} 0 & 0 & 0 \\ 0 & 0 & \beta_1 \\ 0 & -\beta_1 & 0 \end{pmatrix}, \quad [A_8^1] = \begin{pmatrix} 0 & 0 & \beta_1 \\ 0 & 0 & 0 \\ -\beta_1 & 0 & 0 \end{pmatrix} \\
&[A_9^1] = \begin{pmatrix} 0 & 0 & 0 \\ 0 & 0 & 0 \\ -\beta_1 & 0 & 0 \end{pmatrix}, \quad [D_9^1] = \begin{pmatrix} 0 & 0 & 0 \\ 0 & 0 & \frac{d\lambda}{d\theta} \\ 0 & -\frac{d\mu}{d\theta} & 0 \end{pmatrix}.
\end{aligned} \tag{33}$$

The ODE given by equation (32) is complemented by traction free boundary conditions in equation $(17)_2$:

$$\left\{ [B_1^0] \boldsymbol{\varphi}_1' + \left(\alpha [B_2^0] + [B_3^1] \right) \boldsymbol{\varphi}_1 + [B_4^1] \boldsymbol{\varphi}_0 \right\} |_{\theta=0,\omega} = \vec{0}, \tag{34}$$

with

$$[B_3^1] = [B_3^0] + [B_2^0], \quad [B_4^1] = \begin{pmatrix} 0 & 0 & 0 \\ 0 & 0 & \lambda \\ 0 & \frac{1}{2}\mu & 0 \end{pmatrix}. \tag{35}$$

The weak form is obtained by multiplying equation (32) by a test function $\boldsymbol{v}$ and integrating over $0 \leq \theta \leq \omega$, then integrating by parts the second derivative term and substituting equation (34) to apply traction free boundary conditions

$$\begin{aligned} &- \left\{ \left\{ (\alpha[B_2^0] + [B_3^1])\boldsymbol{\varphi}_1 \right\}^{\mathrm{T}} \boldsymbol{v} \right\} |_{\theta=0,\omega} - \left\{ \left\{ [B_4^1]\boldsymbol{\varphi}_0 \right\}^{\mathrm{T}} \boldsymbol{v} \right\} |_{\theta=0,\omega} - \int_0^\omega \left([A_1^0]\boldsymbol{\varphi}_1' \right)^{\mathrm{T}} \boldsymbol{v}' d\theta \\ &+ \int_0^\omega \left[\left(\alpha[A_2^0] + [A_3^1] \right) \boldsymbol{\varphi}_1' \right]^{\mathrm{T}} \boldsymbol{v} d\theta + \int_0^\omega \left[\left(\alpha^2[A_4^0] + \alpha \left([A_5^1] + [D_5^0] \right) + [A_6^1] + [D\,{}_6^1] \right) \boldsymbol{\varphi}_1 \right]^{\mathrm{T}} \boldsymbol{v} d\theta \\ &+ \int_0^\omega \left([A_7^1]\boldsymbol{\varphi}_0' \right)^{\mathrm{T}} \boldsymbol{v} d\theta + \int_0^\omega \left[\left(\alpha[A_8^1] + [A_9^1] + [D_9^1] \right) \boldsymbol{\varphi}_0 \right]^{\mathrm{T}} \boldsymbol{v} d\theta = 0. \end{aligned}$$

The weak formulation for the computation of $\boldsymbol{\varphi}_1$ is

$$\boxed{\begin{array}{c} \text{Seek} \quad \boldsymbol{\varphi}_1 \in H^1(0,\omega), \quad \text{s.t.} \\ \mathcal{B}^1(\boldsymbol{\varphi}_1, \boldsymbol{v}) = \mathcal{F}^1(\boldsymbol{v}), \quad \forall \boldsymbol{v} \in H^1(0,\omega) \end{array}} \tag{36}$$

where H^1 is the Sobolev space

$$\begin{aligned} \mathcal{B}^1(\boldsymbol{\varphi}_1, \boldsymbol{v}) = &-\alpha \left\{ \left\{ [B_2^0]\boldsymbol{\varphi}_1 \right\}^{\mathrm{T}} \boldsymbol{v} \right\} |_{\theta=0,\omega} - \left\{ \left\{ [B_3^1]\boldsymbol{\varphi}_1 \right\}^{\mathrm{T}} \boldsymbol{v} \right\} |_{\theta=0,\omega} \\ &- \int_0^\omega \left([A_1^0]\boldsymbol{\varphi}_1' \right)^{\mathrm{T}} \boldsymbol{v}' d\theta + \int_0^\omega \left[\left(\alpha[A_2^0] + [A_3^1] \right) \boldsymbol{\varphi}_1' \right]^{\mathrm{T}} \boldsymbol{v} d\theta \\ &+ \int_0^\omega \left[\left(\alpha^2[A_4^0] + \alpha \left([A_5^1] + [D_5^0] \right) + [A_6^1] + [D\,{}_6^1] \right) \boldsymbol{\varphi}_1 \right]^{\mathrm{T}} \boldsymbol{v} d\theta \\ \mathcal{F}^1(\boldsymbol{v}) = &\left\{ \left\{ [B_4^1]\boldsymbol{\varphi}_0 \right\}^{\mathrm{T}} \boldsymbol{v} \right\} |_{\theta=0,\omega} - \int_0^\omega \left([A_7^1]\boldsymbol{\varphi}_0' \right)^{\mathrm{T}} \boldsymbol{v} d\theta \\ &- \int_0^\omega \left[\left(\alpha[A_8^1] + [A_9^1] + [D_9^1] \right) \boldsymbol{\varphi}_0 \right]^{\mathrm{T}} \boldsymbol{v} d\theta. \end{aligned} \tag{37}$$

3.2.1. p-FEMs for the first shadow function, $\boldsymbol{\varphi}_1$ We apply p-FEMs for the solution of equation (36) similarly to Subsection 3.1.1. To this end, $\boldsymbol{\varphi}_1 = \begin{pmatrix} u_1 & v_1 & w_1 \end{pmatrix}^{\mathrm{T}} = [N]\boldsymbol{a}_1$ and $\boldsymbol{v} \overset{\text{def}}{=} [N]\boldsymbol{b}_1$. The resulting FE formulation is

$$\boldsymbol{a}_1^{\mathrm{T}}[K^1] = \boldsymbol{F}^1, \tag{38}$$

where

$$\begin{aligned} [K^1] = &- \left\{ [N]^{\mathrm{T}} \left(\alpha[B_2^0]^{\mathrm{T}} + [B_3^1]^{\mathrm{T}} \right) [N] \right\} |_{\theta=0,\omega} \\ &- \frac{2}{\omega} \int_{-1}^{1} [N']^{\mathrm{T}} [A_1^0]^{\mathrm{T}} [N'] d\xi + \int_{-1}^{1} [N']^{\mathrm{T}} \left(\alpha[A_2^0]^{\mathrm{T}} + [A_3^1]^{\mathrm{T}} \right) [N] d\xi \\ &+ \frac{\omega}{2} \int_{-1}^{1} [N]^{\mathrm{T}} \left(\alpha^2[A_4^0]^{\mathrm{T}} + \alpha([A_5^1]^{\mathrm{T}} + [D_5^0]^{\mathrm{T}}) + [A_6^1]^{\mathrm{T}} + [D\,{}_6^1]^{\mathrm{T}} \right) [N] d\xi \\ \boldsymbol{F}^1 = &\left\{ \boldsymbol{a}_0^{\mathrm{T}} [N]^{\mathrm{T}} [B_4^1]^{\mathrm{T}} [N] \right\} |_{\theta=0,\omega} - \int_{-1}^{1} \boldsymbol{a}_0^{\mathrm{T}} [N']^{\mathrm{T}} [A_7^1]^{\mathrm{T}} [N] d\xi \\ &- \frac{\omega}{2} \int_{-1}^{1} \boldsymbol{a}_0^{\mathrm{T}} [N]^{\mathrm{T}} \left(\alpha[A_8^1]^{\mathrm{T}} + [A_9^1]^{\mathrm{T}} + [D_9^1]^{\mathrm{T}} \right) [N] d\xi. \end{aligned} \tag{39}$$

3.3. The jth shadow function, $\boldsymbol{\varphi}_j$, $j \geq 2$. Any shadow and dual functions $\boldsymbol{\varphi}_j$ and $\boldsymbol{\psi}_j$ for $j \geq 2$ can be computed recursively once the shadows $j-1$ and $j-2$ are available by equation $(5)_3$.

Remark 5 *Here we address $\boldsymbol{\varphi}_j$, however $\boldsymbol{\psi}_j$ is computed identically by replacing $\boldsymbol{\varphi}_j$, $\boldsymbol{\varphi}_{j-1}$, $\boldsymbol{\varphi}_{j-2}$ and α by $\boldsymbol{\psi}_j$, $\boldsymbol{\psi}_{j-1}$, $\boldsymbol{\psi}_{j-2}$ and $-\alpha$.*

Substituting $r^{\alpha+j}\boldsymbol{\varphi}_j^{(\alpha)}$ for $\boldsymbol{\Phi}_j$ in equation $(5)_3$ ($j \geq 2$), the dependency on r disappears, and an ODE in θ is obtained

$$[A_1^0]\boldsymbol{\varphi}_2'' + \left(\alpha[A_2^0] + [A_3^j] + [D_3^0]\right)\boldsymbol{\varphi}_2' + \left(\alpha^2[A_4^0] + \alpha([A_5^j] + [D_5^0]) + [A_6^j] + [D^j{}_6]\right)\boldsymbol{\varphi}_j$$
$$+[A_7^1]\boldsymbol{\varphi}_1' + \left(\alpha[A_8^1] + [A_9^j] + [D_9^1]\right)\boldsymbol{\varphi}_{j-1} + [A_{10}^2]\boldsymbol{\varphi}_{j-2} = 0. \tag{40}$$

The matrices $[A_i^j]$ depend on material properties

$$[A_3^j] = [A_3^{j-1}] + [A_2^0], \quad [A_5^j] = [A_5^{j-1}] + 2[A_4^0], \quad [A_6^j] = [A_6^{j-1}] + [A_5^{j-1}] + [A_4^0],$$
$$[D^j{}_6] = [D^{j-1}{}_6] + [D_5^0], \quad [A_9^j] = [A_9^{j-1}] + [A_8^1],$$
$$[A_{10}^2] = \begin{pmatrix} \mu & 0 & 0 \\ 0 & \mu & 0 \\ 0 & 0 & \frac{1}{2}\beta_2 \end{pmatrix}. \tag{41}$$

The ODE given by equation (40) is complemented by traction free boundary conditions in equation $(17)_2$

$$\left\{[B_1^0]\boldsymbol{\varphi}_j' + \left(\alpha[B_2^0] + [B_3^j]\right)\boldsymbol{\varphi}_j + [B_4^1]\boldsymbol{\varphi}_{j-1}\right\}|_{\theta=0,\omega} = \vec{0} \tag{42}$$

with

$$[B_3^j] = [B_3^{j-1}] + [B_2^0]. \tag{43}$$

Following the same steps as in Section 3.2, we obtain the weak form for the function $\boldsymbol{\varphi}_j$

$$\boxed{\begin{array}{c} \text{Seek} \quad \boldsymbol{\varphi}_j \in H^1(0,\omega), \quad \text{s.t.} \\ \mathcal{B}^j(\boldsymbol{\varphi}_j, \boldsymbol{v}) = \mathcal{F}^j(\boldsymbol{v}), \quad \forall \boldsymbol{v} \in H^1(0,\omega) \end{array}} \tag{44}$$

where

$$\mathcal{B}^j(\boldsymbol{\varphi}_j, \boldsymbol{v}) = -\alpha\left\{\left\{[B_2^0]\boldsymbol{\varphi}_j\right\}^{\mathrm{T}}\boldsymbol{v}\right\}|_{\theta=0,\omega} - \left\{\left\{[B_3^j]\boldsymbol{\varphi}_j\right\}^{\mathrm{T}}\boldsymbol{v}\right\}|_{\theta=0,\omega}$$
$$-\int_0^\omega \left([A_1^0]\boldsymbol{\varphi}_j'\right)^{\mathrm{T}}\boldsymbol{v}'d\theta + \int_0^\omega \left[\left(\alpha[A_2^0] + [A_3^j] + [D_3^0]\right)\boldsymbol{\varphi}_j'\right]^{\mathrm{T}}\boldsymbol{v}d\theta$$
$$+\int_0^\omega \left[\left(\alpha^2[A_4^0] + \alpha\left([A_5^j] + [D_5^0]\right) + [A_6^j] + [D^j{}_6]\right)\boldsymbol{\varphi}_j\right]^{\mathrm{T}}\boldsymbol{v}d\theta$$
$$\mathcal{F}^j(\boldsymbol{v}) = \left\{\left\{[B_4^1]\boldsymbol{\varphi}_{j-1}\right\}^{\mathrm{T}}\boldsymbol{v}\right\}|_{\theta=0,\omega} - \int_0^\omega \left([A_7^1]\boldsymbol{\varphi}_{j-1}'\right)^{\mathrm{T}}\boldsymbol{v}d\theta$$
$$-\int_0^\omega \left[\left(\alpha[A_8^1] + [A_9^j] + [D_9^1]\right)\boldsymbol{\varphi}_{j-1}\right]^{\mathrm{T}}\boldsymbol{v}d\theta - \int_0^\omega \left([A_{10}^2]\boldsymbol{\varphi}_{j-2}\right)^{\mathrm{T}}\boldsymbol{v}d\theta. \tag{45}$$

3.3.1 p-FEMs for the jth shadow function, $\boldsymbol{\varphi}_j$. p-FEMs for the solution of equation (44) are similar to Subsection 3.2.1. To this end $\boldsymbol{\varphi}_j = \begin{pmatrix} u_j & v_j & w_j \end{pmatrix}^{\mathrm{T}} = [N]\boldsymbol{a}_j$ and $\boldsymbol{v} \overset{\text{def}}{=} [N]\boldsymbol{b}_j$. The resulting FE formulation is

$$\boldsymbol{a}_j^{\mathrm{T}}[K^j] = \boldsymbol{F}^j, \tag{46}$$

where

$$
\begin{aligned}
[K^j] = &-\left\{[N]^{\mathrm{T}}\left(\alpha[B_2^0]^{\mathrm{T}} + [B_3^2]^{\mathrm{T}}\right)[N]\right\}|_{\theta=0,\omega} \\
&-\frac{2}{\omega}\int_{-1}^{1}[N']^{\mathrm{T}}[A_1^0]^{\mathrm{T}}[N']d\xi + \int_{-1}^{1}[N']^{\mathrm{T}}\left(\alpha[A_2^0]^{\mathrm{T}} + [A_3^j]^{\mathrm{T}} + [D_3^0]^{\mathrm{T}}\right)[N]d\xi \\
&+\frac{\omega}{2}\int_{-1}^{1}[N]^{\mathrm{T}}\left(\alpha^2[A_4^0]^{\mathrm{T}} + \alpha([A_5^j]^{\mathrm{T}} + [D_5^0]^{\mathrm{T}}) + [A_6^j]^{\mathrm{T}} + [D^j{}_6]^{\mathrm{T}}\right)[N]d\xi \\
\boldsymbol{F}^j = &\left\{\boldsymbol{a}_{j-1}^{\mathrm{T}}[N]^{\mathrm{T}}[B_4^1]^{\mathrm{T}}[N]\right\}|_{\theta=0,\omega} - \int_{-1}^{1}\boldsymbol{a}_{j-1}^{\mathrm{T}}[N']^{\mathrm{T}}[A_7^1]^{\mathrm{T}}[N]d\xi \\
&-\frac{\omega}{2}\int_{-1}^{1}\boldsymbol{a}_{j-1}^{\mathrm{T}}[N]^{\mathrm{T}}\left(\alpha[A_8^1]^{\mathrm{T}} + [A_9^j]^{\mathrm{T}} + [D_9^1]^{\mathrm{T}}\right)[N]d\xi - \frac{\omega}{2}\int_{-1}^{1}\boldsymbol{a}_{j-2}^{\mathrm{T}}[N]^{\mathrm{T}}[A_{10}^2]^{\mathrm{T}}[N]d\xi.
\end{aligned}
$$

4. Numerical example

Four example problems, for which the eigenpairs, shadows and duals are computed by applying p-FEMs, are presented. The relative error in percentage of the computed eigenvalues α_i is defined by

$$
\%\text{error}(\alpha_i^{(p)}) = 100\left|\frac{\alpha_i^{(p)} - \alpha_i^{(p_{\max})}}{\alpha_i^{(p_{\max})}}\right|, \tag{47}
$$

where p refers to the p-level of the FE solution.

Remark 6 *The eigen-pairs in the examples presented herein are numbered according to their affiliation to fracture mechanics classic Modes (Mode I, Mode II, Mode III) and not enumerated by increasing order.*

4.1. A cracked domain with symmetric material properties $E(\theta) = \frac{1}{\pi^2}(3\pi^2 - 2\pi\theta + \theta^2)$

We consider a 3-D domain having a crack ($\omega = 2\pi$) with its tip along the x_3 axis. We select a constant Poisson ratio $\nu = 0.3$ and a Young's modulus that is a symmetric function of θ:

$$
E(\theta) = \frac{1}{\pi^2}(3\pi^2 - 2\pi\theta + \theta^2), \tag{48}
$$

as shown in Figure 2. The Lamè functions of θ are

$$
\lambda(\theta) = \frac{15}{26\pi^2}(3\pi^2 - 2\pi\theta + \theta^2), \qquad \mu(\theta) = \frac{5}{13\pi^2}(3\pi^2 - 2\pi\theta + \theta^2). \tag{49}
$$

We use two equal finite elements and 54 Gauss integration points to compute the first three eigenpairs, obtaining at $p = 16$ (204 degrees of freedom (DOFs))

$$
\alpha_1^{(16)} = 0.45628417, \qquad \alpha_2^{(16)} = 0.48058596, \qquad \alpha_3^{(16)} = 0.45796492. \tag{50}
$$

We demonstrate the convergence of the results by plotting the relative error as a function of the number of degrees of freedom in the FE analysis for α_1, α_2, α_3 in Figure 3. An exponential convergence rate is noticed as expected. Of course that for constant material properties the three eigenvalues were $\alpha_1 = \alpha_2 = \alpha_3 = \frac{1}{2}$. One thus observes that the eigenvalues obtained are smaller than $\frac{1}{2}$ and the solution is therefore more singular compared to the "usual crack". This is because the Young's modulus is larger at the crack edges ($\theta = 0, 2\pi$) and smaller at the middle (at $\theta = \pi$).

The eigenfunctions and first two shadows associated with the first three eigenvalues are presented in Figures 4 to 6. The first two eigenvalues are associated with the in-plane displacements where $w_0 \equiv 0$ and the third eigenvalue is associated with the perpendicular displacement, where u_0 and v_0 are identically zero.

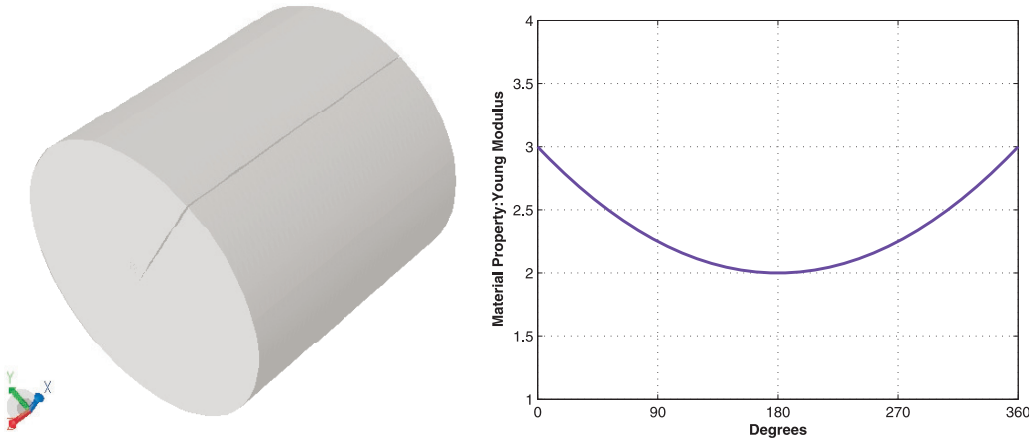

Figure 2. Left: The considered cracked domain. Right: Symmetric Young's modulus as a function of θ.

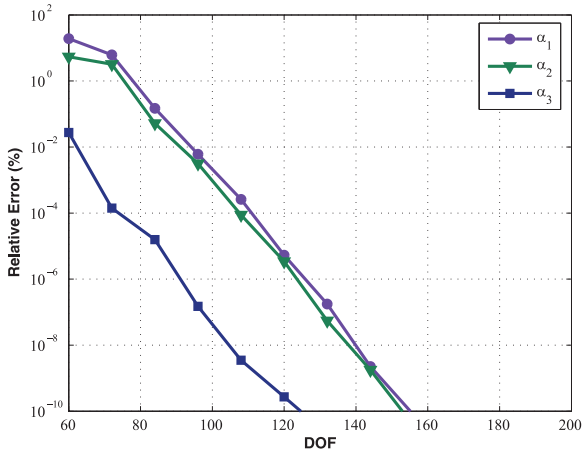

Figure 3. Relative error of eigenvalues α_1, α_2, α_3, for a cracked domain with traction free boundary conditions. $E(\theta) = \frac{1}{\pi^2}(3\pi^2 - 2\pi\theta + \theta^2)$, $\nu = 0.3$.

4.2. A V-Notched domain ($\omega = \frac{3\pi}{2}$) with $E(\theta) = 3 - \frac{4}{\pi}\theta + \frac{16}{3\pi^2}\theta^2 - \frac{64}{27\pi^3}\theta^3$

Similar to the previous subsection, we consider a traction-free domain having a V-notch ($\omega = \frac{3\pi}{2}$) with the edge along the x_3 axis (see Figure 7). We select the Young's modulus to be a asymmetric function along θ and Poisson Ratio to be $\nu = 0.3$ (see Figure 7)

$$E(\theta) = 3 - \frac{4}{\pi}\theta + \frac{16}{3\pi^2}\theta^2 - \frac{64}{27\pi^3}\theta^3, \qquad \nu = 0.3. \tag{51}$$

The Lamè functions are

$$\lambda(\theta) = \frac{15}{26}\left(3 - \frac{4}{\pi}\theta + \frac{16}{3\pi^2}\theta^2 - \frac{64}{27\pi^3}\theta^3\right), \qquad \mu(\theta) = \frac{15}{13}\left(3 - \frac{4}{\pi}\theta + \frac{16}{3\pi^2}\theta^2 - \frac{64}{27\pi^3}\theta^3\right). \tag{52}$$

Using two equal finite elements and 54 Gauss integration points, we compte the first three eigenpairs at $p = 16$ (204 DOFs)

$$\alpha_1^{(16)} = 0.55293099, \qquad \alpha_2^{(16)} = 0.92779656, \qquad \alpha_3^{(16)} = 0.67494905 \tag{53}$$

The relative errors for $\alpha_1, \alpha_2, \alpha_3$ as a function of the number of degrees of freedom in the FE analysis are plotted in Figure 8. As expected, exponential convergence rate is noticed.

The eigenfunctions and first two shadows related with the first three eigenvalues are shown in Figures 9 to 11. Similar to the example presented in Subsection 4.1, the first two eigenvalues are associated with the in-plane

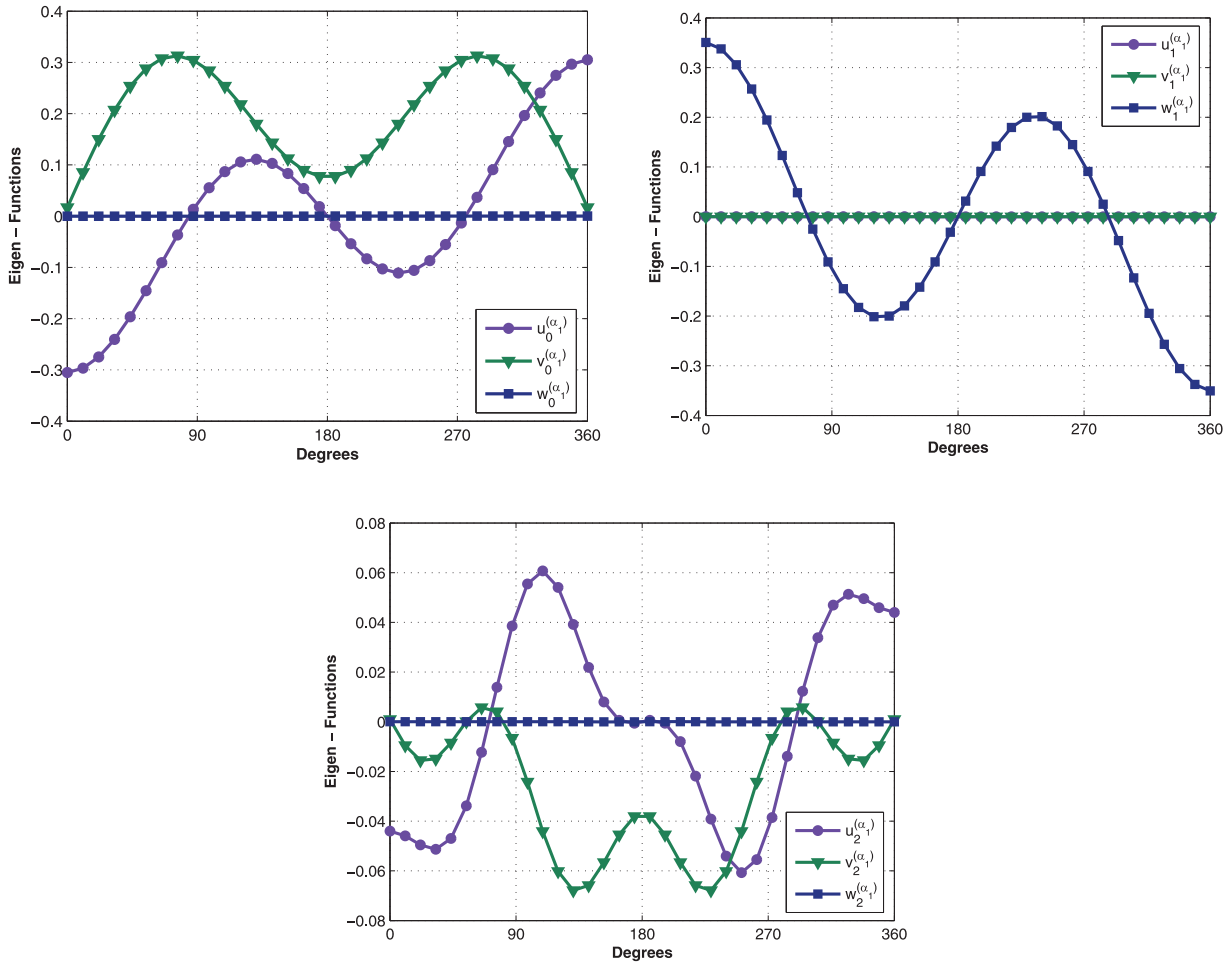

Figure 4. The eigenfunctions u, v, w associated with $\varphi_0, \varphi_1, \varphi_2$ of the first eigenvalue, $\alpha_1 = 0.456284$, for cracked domain with traction free boundary conditions. ($E(\theta) = \frac{1}{\pi^2}(3\pi^2 - 2\pi\theta + \theta^2)$, $\nu = 0.3$). Top Left: the eigenfunction φ_0. Top Right: the first shadow function φ_1. Bottom: the second shadow function φ_2.

displacements and the third eigenvalue is associated with the perpendicular displacement. It may be observed that the eigenfunctions, as well as the shadow functions, are neither symmetric nor asymmetric function, due to the asymmetric material properties in the presented example and therefore the two in-plane solutions (related with α_1, α_2) may not be separated in to Mode *I* and Mode *II* as is customarily performed in fracture mechanics.

4.3. A cracked domain with $E(\theta) = \frac{1}{\pi^2}(1 - 2\pi\theta + 3\pi^2\theta^2)$

Consider a 3-D domain having a crack ($\omega = 2\pi$) with its tip along the x_3 axis. Consider a constant Poisson ratio $\nu = 0.3$ and a Young's modulus that is a non-symmetric function of θ:

$$E(\theta) = \frac{1}{\pi^2}(1 - 2\pi\theta + 3\pi^2\theta^2), \tag{54}$$

as shown in Figure 12. The Lamè functions are

$$\lambda(\theta) = \frac{15}{26\pi^2}(1 - 2\pi\theta + 3\pi^2\theta^2), \qquad \mu(\theta) = \frac{5}{13\pi^2}(1 - 2\pi\theta + 3\pi^2\theta^2). \tag{55}$$

We use two equal finite elements and 54 Gauss integration points to compute the first three eigenpairs, obtaining at $p = 16$ (204 DOFs)

$$\alpha_1^{(16)} = 0.64685702, \qquad \alpha_2^{(16)} = 0.77802188, \qquad \alpha_3^{(16)} = 0.72514129. \tag{56}$$

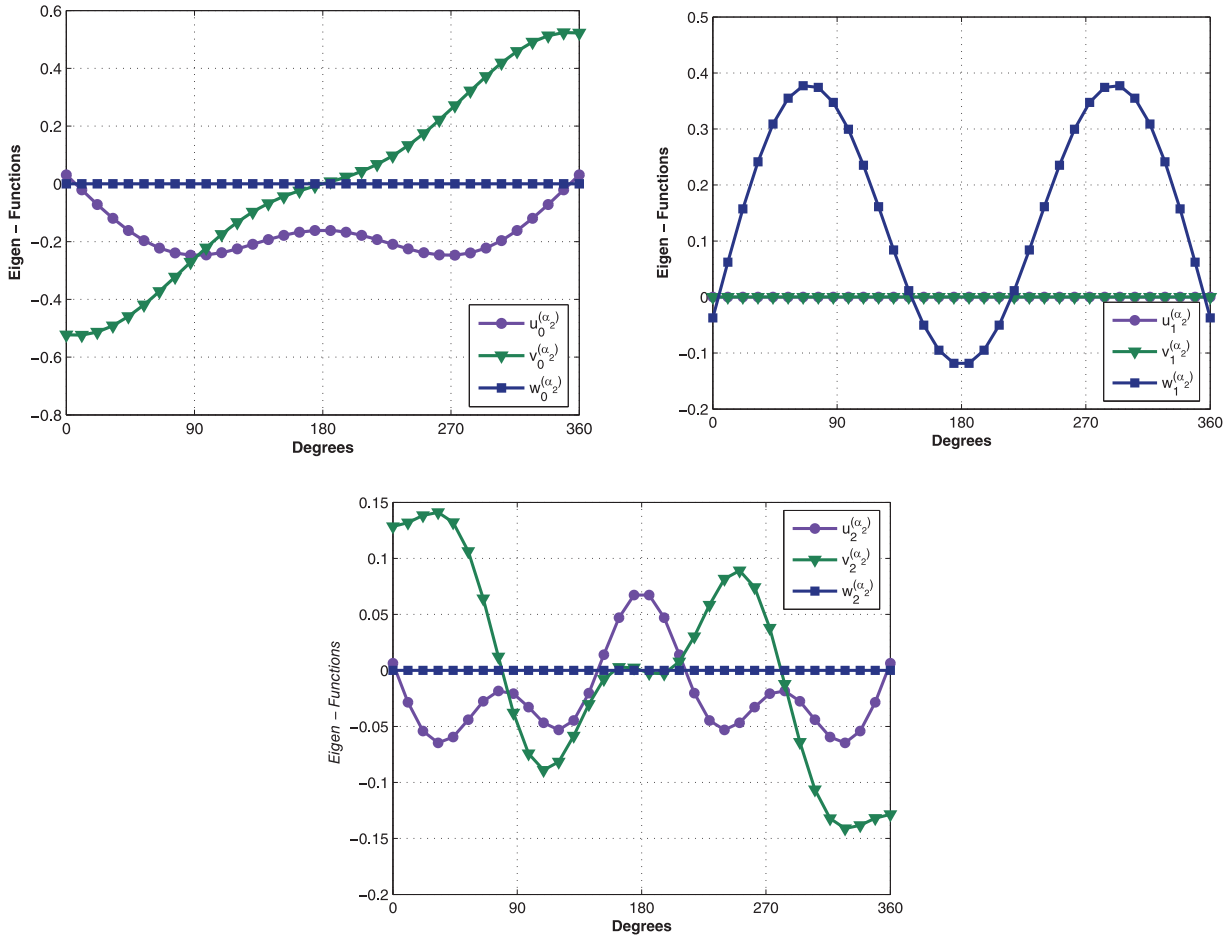

Figure 5. The eigenfunctions u, v, w associated with $\varphi_0, \varphi_1, \varphi_2$ of the second eigenvalue, $\alpha_2 = 0.480586$, for cracked domain with traction free boundary conditions. ($E(\theta) = \frac{1}{\pi^2}(3\pi^2 - 2\pi\theta + \theta^2)$, $\nu = 0.3$). Top Left: the eigenfunction φ_0. Top Right: the first shadow function φ_1. Bottom: the second shadow function φ_2.

The convergence of the eigenvalues $\alpha_1, \alpha_2, \alpha_3$ is shown in Figure 13.

Comparing the obtained eigenvalues to the first three eigenvalues for an isotropic domain, which are $\alpha_1 = \alpha_2 = \alpha_3 = \frac{1}{2}$, we may conclude that the chosen θ-varying Young's modulus considerably increases the values of these eigenvalues, thus the solution is considerably less singular.

The eigenfunctions and first two shadows associated with the first three eigenvalues are shown in Figures 14 to 16.

The Top left graphs of Figures 14 to 16 show the eigenfunction φ_0 associated with the eigenvalues $\alpha_1 - \alpha_3$. One may notice that the first two eigenvalues are associated with the in-plane displacements where w_0 is identically zero. The third eigenvalue is associated with the perpendicular displacement where u_0 and v_0 are identically zero. Furthermore, these eigenvalues are no longer identical to 1/2 as expected when constant material properties are addressed. One may not anymore separate the two in-plane modes into opening and shearing classical modes.

4.4. Sensitivity analysis – difference between a constant E and a varying $E(\theta)$

To investigate the sensitivity of the eigenvalues to the material properties, we consider a 3-D domain having a crack ($\omega = 2\pi$) with its tip along the x_3 axis. The material properties selected are

$$E = S - \frac{2}{\pi}(S-2)\theta + \frac{1}{\pi^2}(S-2)\theta^2, \qquad \nu = 0.3, \tag{57}$$

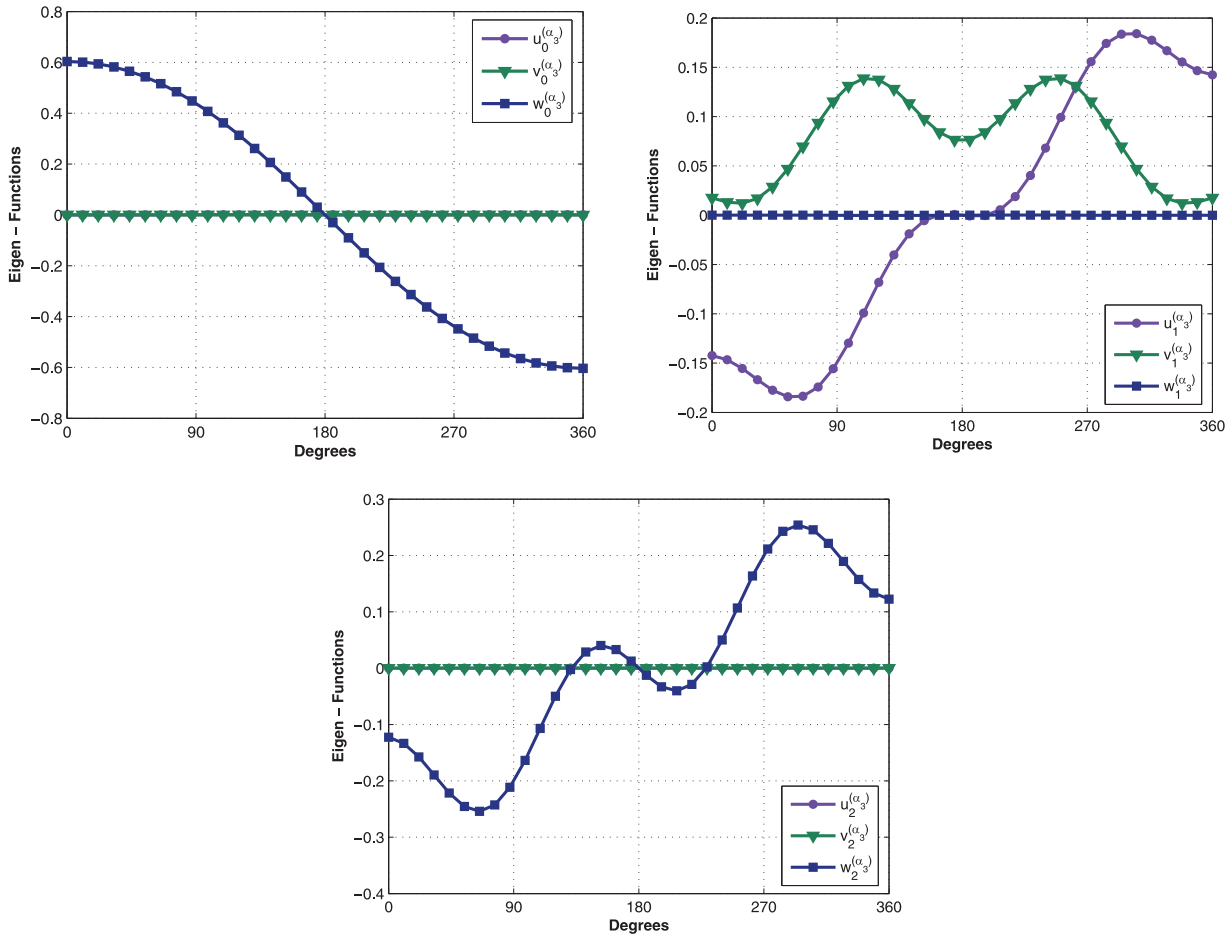

Figure 6. The eigenfunctions u, v, w associated with $\varphi_0, \varphi_1, \varphi_2$ of the third eigenvalue, $\alpha_3 = 0.457965$, for cracked domain with traction free boundary conditions. ($E(\theta) = \frac{1}{\pi^2}(3\pi^2 - 2\pi\theta + \theta^2)$, $\nu = 0.3$). Top Left: the eigenfunction φ_0. Top Right: the first shadow function φ_1. Bottom: the second shadow function φ_2.

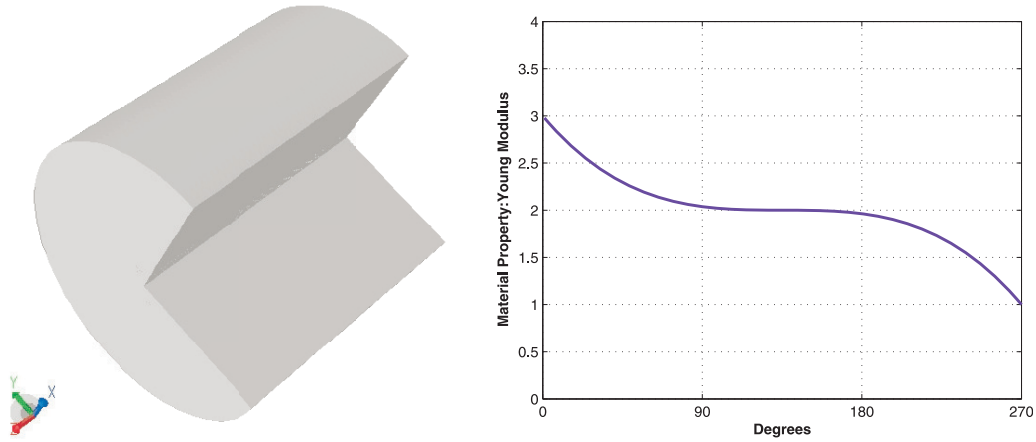

Figure 7. Left: The considered V-noched domain. Right: Young's modulus as a function of θ.

where the Young's modulus is a symmetric function and $S \geq 2$. By selecting $S = 2$ a constant Young's modulus is obtained and by selecting $S = 3$ the example presented herein is reduced to the example presented in Section 4.1. The domain and the Young's modulus are presented in Figure 17 for selected values of S.

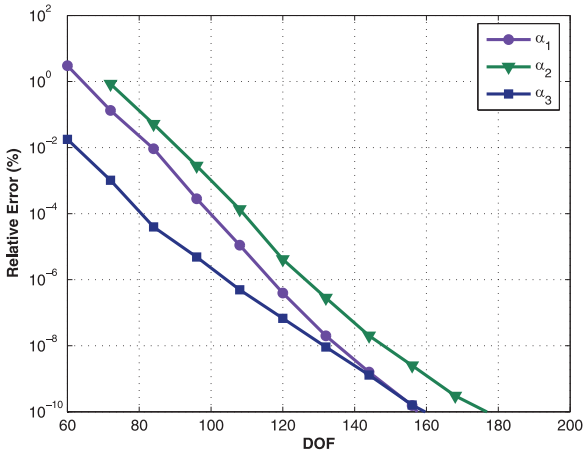

Figure 8. Relative error of eigenvalues $\alpha_1, \alpha_2, \alpha_3$, for a V-notched domain with traction free boundary conditions. $E(\theta) = 3 - \frac{4}{\pi}\theta + \frac{16}{3\pi^2}\theta^2 - \frac{64}{27\pi^3}\theta^3, \quad \nu = 0.3.$

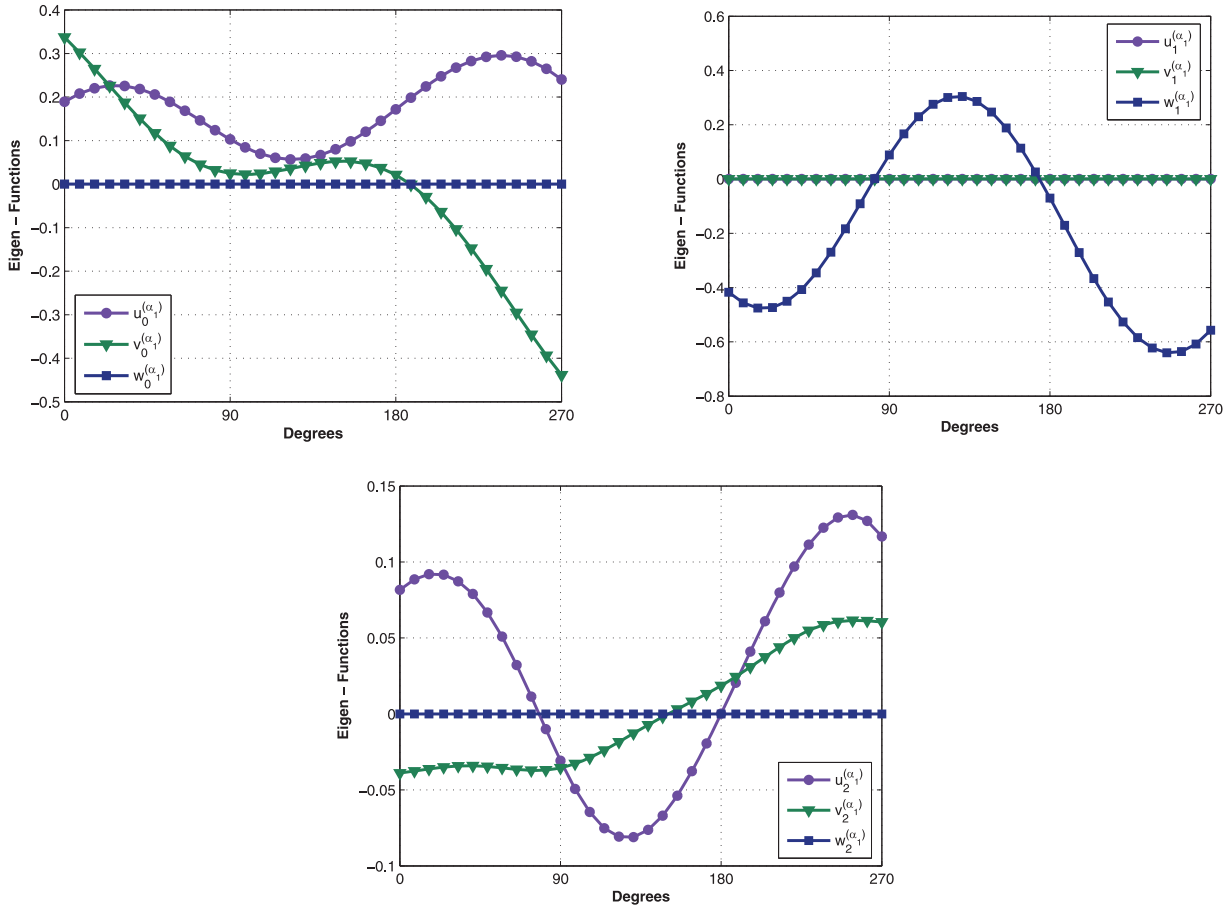

Figure 9. The eigenfunctions u, v, w associated with $\varphi_0, \varphi_1, \varphi_2$ of the first eigenvalue, $\alpha_1 = 0.552931$, for v-notched domain with traction free boundary conditions. ($E(\theta) = 3 - \frac{4}{\pi}\theta + \frac{16}{3\pi^2}\theta^2 - \frac{64}{27\pi^3}\theta^3, \quad \nu = 0.3$). Top Left: The eigenfunction φ_0. Top Right: The first shadow function φ_1. Bottom: The second shadow function φ_2.

We plotted the first three eigenvalues computed using increasing values of S as shown in Figure 18. As S increases, the values of the Young's modulus located at the crack edges ($\theta = 0, 2\pi$) increases and the solution becomes highly singular (lower values of the eigenvalues are obtained).

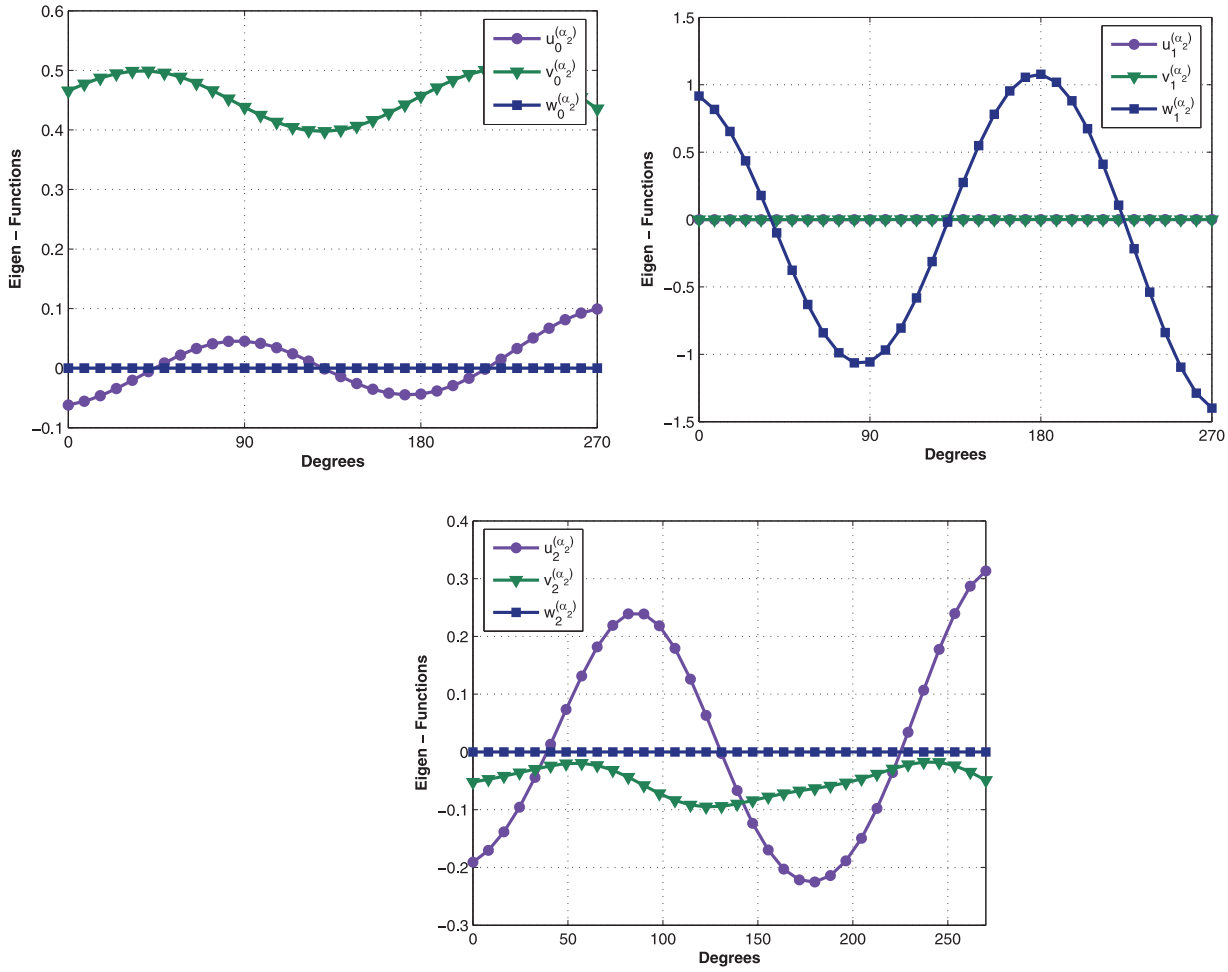

Figure 10. The eigenfunctions u, v, w associated with $\varphi_0, \varphi_1, \varphi_2$ of the second eigenvalue, $\alpha_2 = 0.927797$, for v-notched domain with traction free boundary conditions. ($E(\theta) = 3 - \frac{4}{\pi}\theta + \frac{16}{3\pi^2}\theta^2 - \frac{64}{27\pi^3}\theta^3, \quad \nu = 0.3$). Top Left: The eigenfunction φ_0. Top Right: The first shadow function φ_1. Bottom: The second shadow function φ_2.

5. Summary and conclusions

The asymptotic expansion of the displacements for an isotropic 3-D elastic domain in the vicinity of an edge has been extended to the case where the material properties depend on the angular axis, θ. We derived the weak formulation for the computation of the eigenvalues, eigenfunctions and shadow functions and discretized it using high-order FE methods. The numerical examples are shown to converge exponentially up to less than $10^{-8}\%$ relative error.

In the case of a single material domain, having constant material properties, the eigenvalues are independent of the selection of material constants. However herein, the numerical examples demonstrate that the eigenpairs depend on angular variation of the material properties. For different choices of angular variations of the Young's modulus the singularity of the solution may be either more or less severe compared to constant material properties.

For the important cracked-domain having $\alpha = \frac{1}{2}$ for constant material properties, we observed that varying the Young's modulus in the angular direction results in different eigenvalues. Although the first two eigenpairs are associated with the in-plane displacements and the third is associated with the perpendicular displacement, the eigenfunctions as well as the shadow functions are no longer symmetric nor asymmetric functions and therefore Mode *I* and Mode *II* may no longer be separated, as customary in conventional fracture mechanics.

The methods presented were shown to be accurate and efficient.

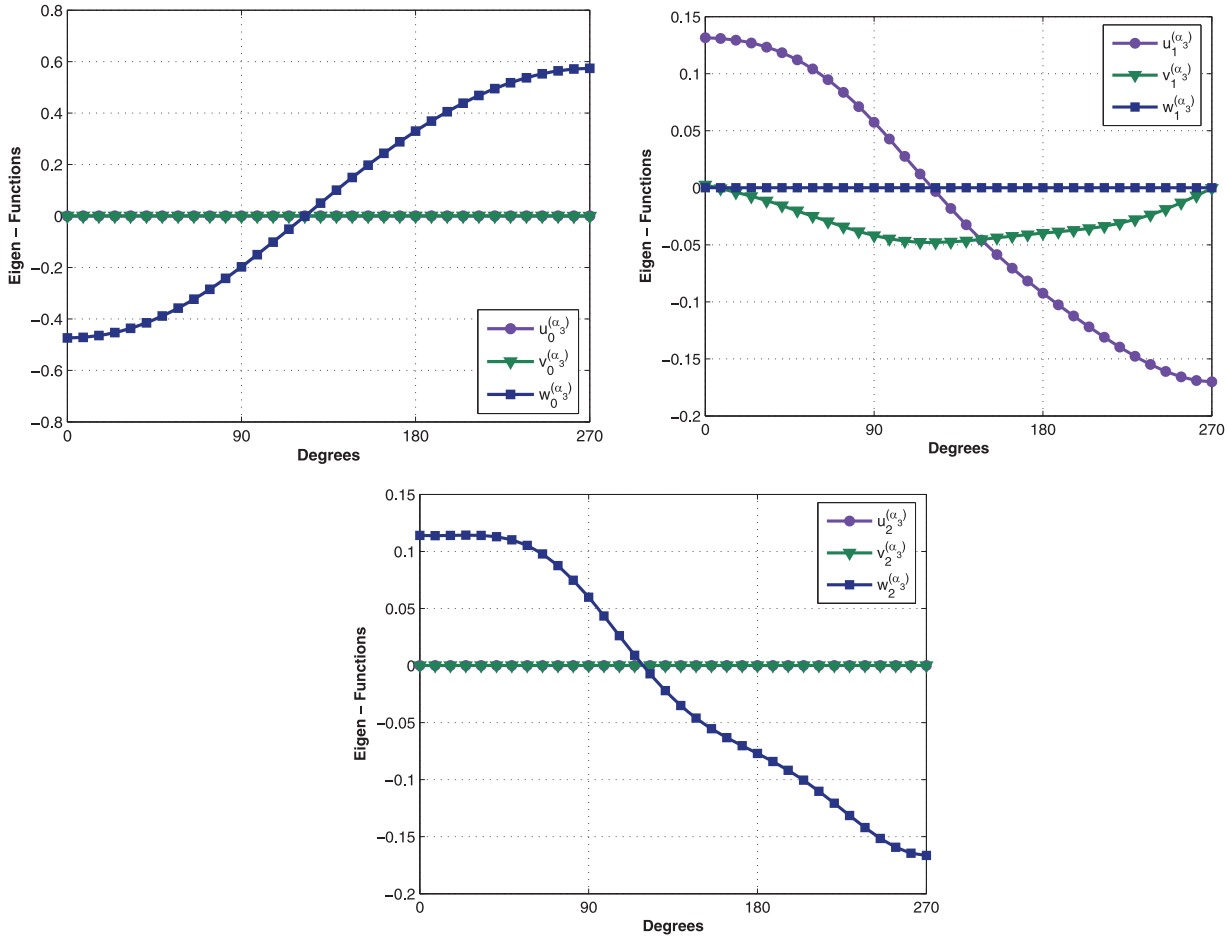

Figure 11. The eigenfunctions u, v, w associated with $\varphi_0, \varphi_1, \varphi_2$ of the third eigenvalue, $\alpha_3 = 0.674949$, for v-notched domain with traction free boundary conditions. ($E(\theta) = 3 - \frac{4}{\pi}\theta + \frac{16}{3\pi^2}\theta^2 - \frac{64}{27\pi^3}\theta^3, \quad \nu = 0.3$). Top Left: The eigenfunction φ_0. Top Right: The first shadow function φ_1. Bottom: The second shadow function φ_2.

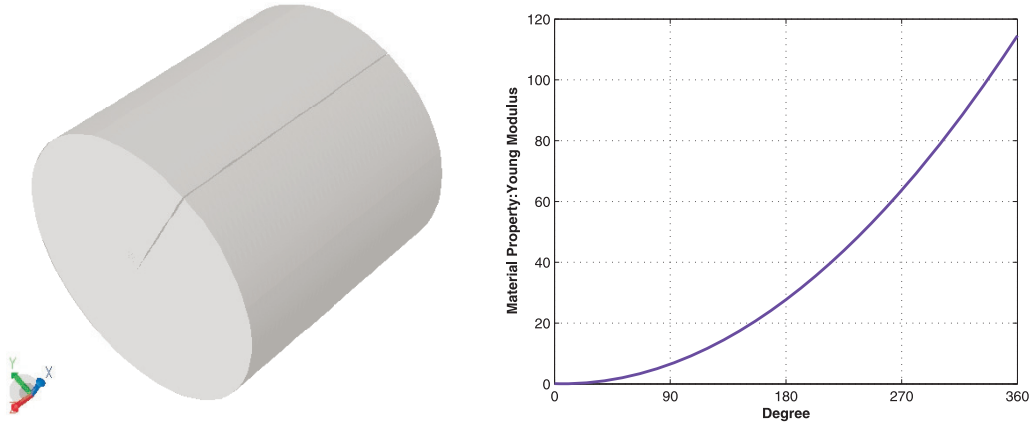

Figure 12. Left: The considered cracked domain. Right: Young's modulus as a function of θ.

The edge stress intensity functions (ESIF) may be extracted using the quasi dual function method (QDFM). The method can be interpreted as an extension of the dual function extraction method in 2-D and its theoretical details were first introduced by Costabel et al. [17]. The method involves the computation of a surface integral $J[R]$ along a cylindrical surface of radius R away from the edge. The $J[R]$ integral utilizes special constructed extraction polynomials together with the dual eigenfunctions for the extraction of the ESIF. The

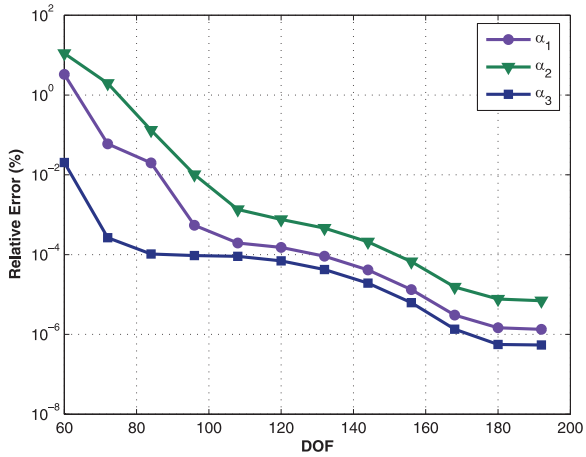

Figure 13. Relative error of eigenvalues α_1, α_2, α_3, for a cracked domain with traction free boundary conditions. $E(\theta) = \frac{1}{\pi^2}(1 - 2\pi\theta + 3\pi^2\theta^2)$, $\nu = 0.3$.

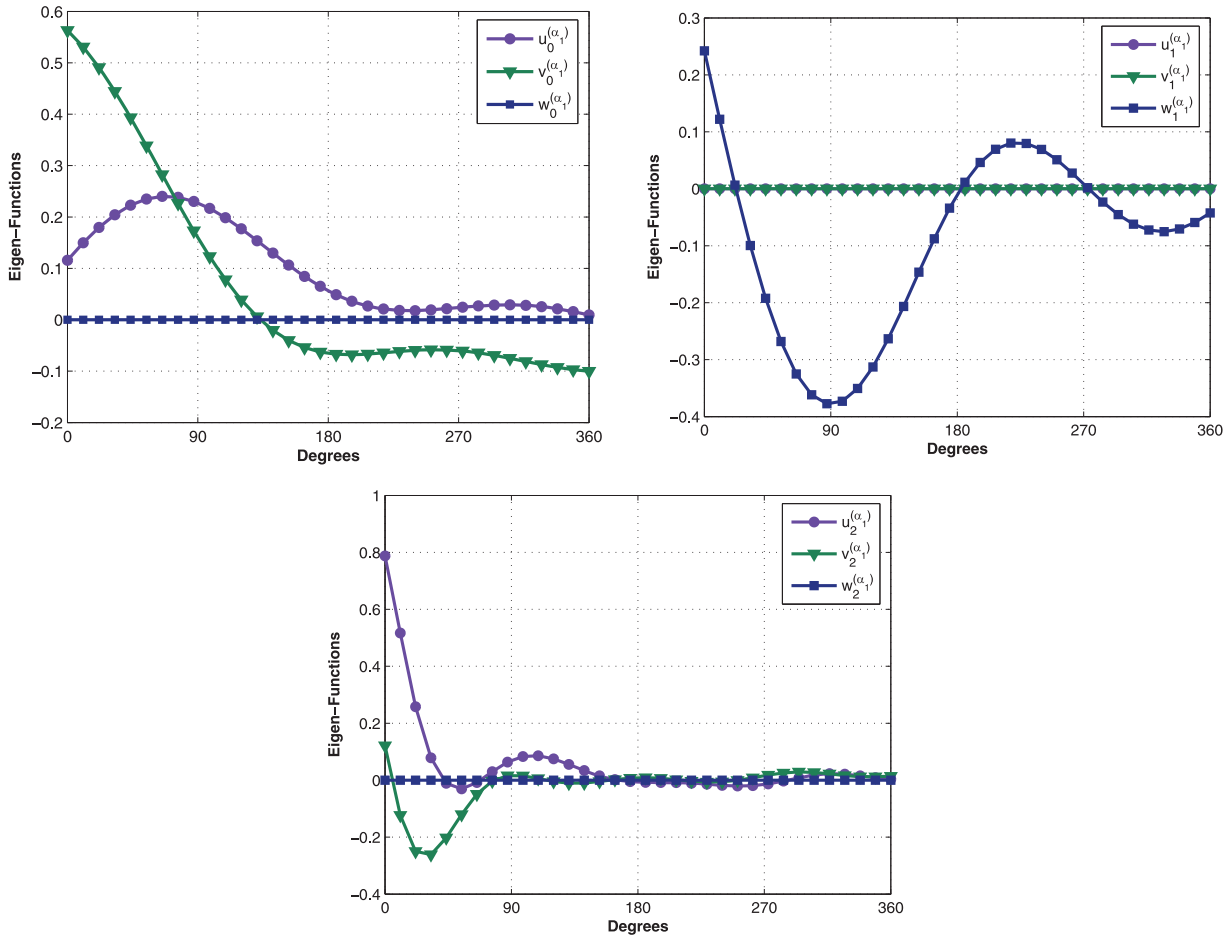

Figure 14. The eigenfunctions u, v, w associated with $\boldsymbol{\varphi}_0, \boldsymbol{\varphi}_1, \boldsymbol{\varphi}_2$ of the first eigenvalue $\alpha_1 = 0.646856$, for cracked domain with traction free boundary conditions. ($E(\theta) = \frac{1}{\pi^2}(1 - 2\pi\theta + 3\pi^2\theta^2)$, $\nu = 0.3$). Top Left: The eigenfunction $\boldsymbol{\varphi}_0$. Top Right: The first shadow function $\boldsymbol{\varphi}_1$. Bottom: The second shadow function $\boldsymbol{\varphi}_2$.

method has been shown to produce accurate results for homogeneous isotropic domains and for homogeneous anisotropic domains by Yosibash et al. [3, 18]. The extension of the QDFM to θ dependent inhomogeneous material properties will be reported in a forthcoming publication.

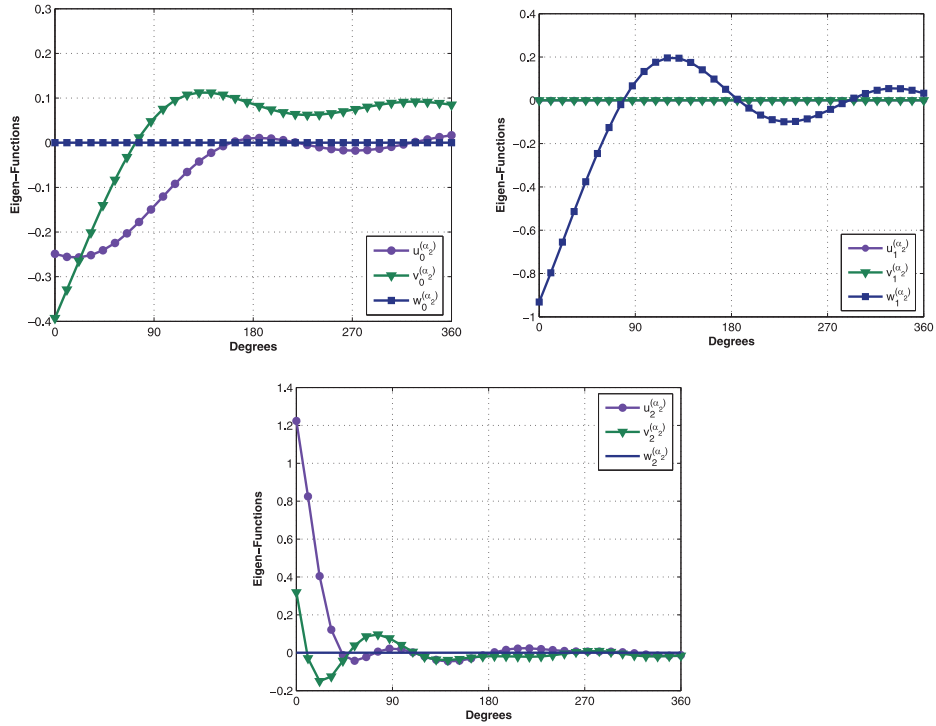

Figure 15. The eigenfunctions u, v, w associated with $\boldsymbol{\varphi}_0, \boldsymbol{\varphi}_1, \boldsymbol{\varphi}_2$ of the second eigenvalue $\alpha_2 = 0.77803$, for cracked domain with traction free boundary conditions. ($E(\theta) = \frac{1}{\pi^2}(1 - 2\pi\theta + 3\pi^2\theta^2)$, $\nu = 0.3$). Top Left: The eigenfunction $\boldsymbol{\varphi}_0$. Top Right: The first shadow function $\boldsymbol{\varphi}_1$. Bottom: The second shadow function $\boldsymbol{\varphi}_2$.

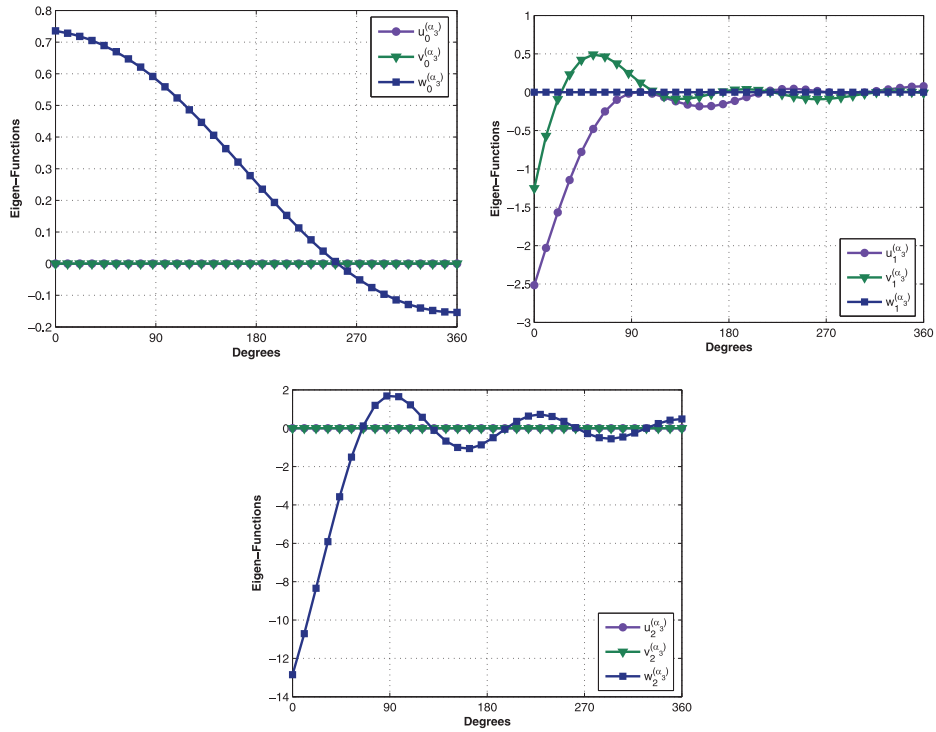

Figure 16. The eigenfunctions u, v, w associated with Φ_0, Φ_1, Φ_2 of the third eigenvalue $\alpha_3 = 0.725142$, for cracked domain with traction free boundary conditions. ($E(\theta) = \frac{1}{\pi^2}(1 - 2\pi\theta + 3\pi^2\theta^2)$, $\nu = 0.3$). Top Left: The eigenfunction $\boldsymbol{\varphi}_0$. Top Right: The first shadow function $\boldsymbol{\varphi}_1$. Bottom: The second shadow function $\boldsymbol{\varphi}_2$.

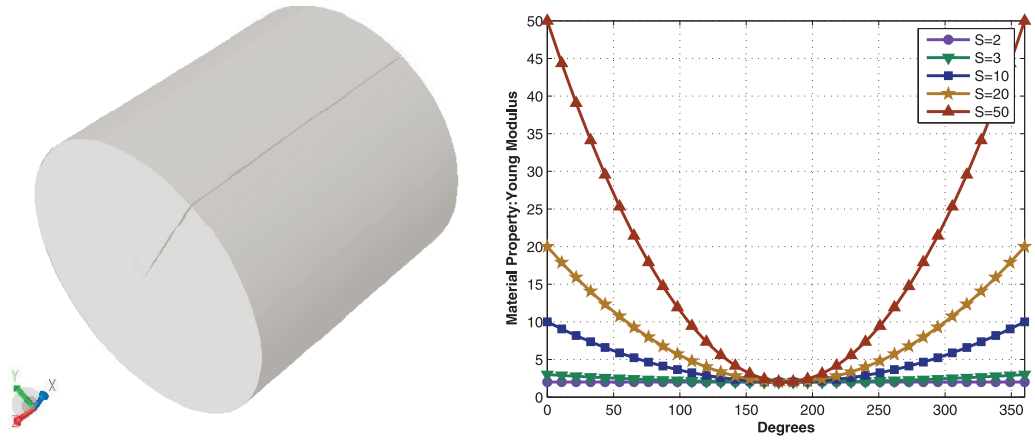

Figure 17. Left: The considered cracked domain. Right: Symmetric Young's modulus as a function of θ presented for selected values of S.

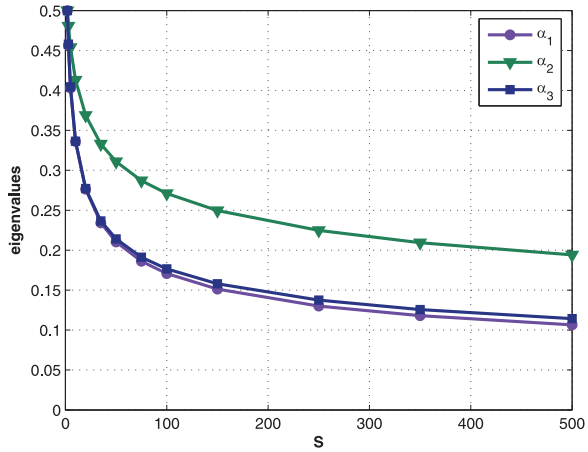

Figure 18. The eigenvalues α_1, α_2, α_3 as a function of S for a cracked domain with traction free boundary conditions. $E = S - \frac{2}{\pi}(S-2)\theta + \frac{1}{\pi^2}(S-2)\theta^2, \quad \nu = 0.3.$

Funding

The author(s) disclosed receipt of the following financial support for the research, authorship, and/or publication of this article: This work was supported by the Israel Science Foundation (grant number 593/14).

References

[1] Omer, N, and Yosibash, Z. Edge singularities in 3-D elastic anisotropic and multi-material domains. *Comput Methods Appl Mech Eng* 2008; 197: 959–978.

[2] Yosibash, Z, Omer, N, and Dauge, M. Edge stress intensity functions in 3-D anisotropic composites. *Compos Sci Technol* 2008; 68: 1216–1224.

[3] Yosibash, Z, and Omer, N. Numerical methods for extracting edge stress intensity functions in anisotropic three-dimensional domains. *Comput Methods Appl Mech Eng* 2007; 196: 3624–3649.

[4] Williams, ML. Stress singularities resulting from various boundary conditions in angular corners of plates in extension. *Trans ASME, Jour Appl Mech* 1952; 19: 526–528.

[5] Karp, S, and Karal, FJ. The elastic field behavior in the neighborhood of a crack of arbitraty angle. *Commun Pure Appl Math* 1962; 15: 413–421.

[6] Grisvard, P. *Elliptic problems in nonsmooth domains*. England: Pitman Publishing, 1985.

[7] Beagles, A, and Sändig, AM. Singularities of rotationally symmetric solutions of boundary value problems for the Lamé equations. *ZAMM - Z Angew Math Mech* 1991; 71: 423–431.

[8] Costabel, M, Dauge, M, and Lafranche, Y. Fast semi-analytic computation of elastic edge singularities. *Comput Methods Appl Mech Eng* 2001; 190: 2111–2134.

[9] Leguillon, D, and Sanchez-Palencia, E. *Computation of singular solutions in elliptic problems and elasticity*. New York: John Wiley & Sons, 1987.
[10] Szabó, BA, and Yosibash, Z. Numerical analysis of singularities in two-dimensions. Part 2: Computation of the generalized flux/stress intensity factors. *Int J Numer Methods Eng* 1996; 39(3): 409–434.
[11] Yosibash, Z, and Szabó, BA. Numerical analysis of singularities in two-dimensions. Part 1: Computation of eigenpairs. *Int J Numer Methods Eng* 1995; 38: 2055–2082.
[12] Yosibash, Z. *Singularities in elliptic boundary value problems and elasticity and their connection with failure initiation*. Springer, New York, USA 2012.
[13] Pook, LP. A 50-year retrospective review of three-dimensional effects at cracks and sharp notches. *Fatigue Fract Eng M* 2013; 36: 699–723.
[14] Rössle, A. Corner singularities and regularity of weak solutions for the two-dimensional Lamé equations on domains with angular corners. *J Elast* 2000; 60: 57–75.
[15] Vasilopoulos, D. On the determination of higher order terms of singular elastic stress fields near corners. *Numer Math* 1988; 53: 51–95.
[16] Szabó, BA, and Babuška, I. *Finite Element Analysis*. New York: John Wiley & Sons, 1991.
[17] Costabel, M, Dauge, M, and Yosibash, Z. A quasidual function method for extracting edge stress intensity functions. *SIAM J Math Anal* 2004; 35: 1177–1202.
[18] Yosibash, Z, Omer, N, Costabel, M, et al. Edge stress intensity functions in polyhedral domains and their extraction by a quasidual function method. *Int J Fracture* 2005; 136: 37–73.
[19] Apel, T, Mehrmann, V, and Watkins, D. Structured eigenvalue method for computation of corner singularities in 3D anisotropic elastic structures. *Comput Methods Appl Mech Eng* 2002; 191: 4459–4473.